Additive Manufacturing 35 (2020) 101177

Contents lists available at ScienceDirect

Additive Manufacturing

journal homepage: www.elsevier.com/locate/addma

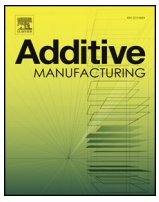

Review

A comprehensive review of the photopolymerization of ceramic resins used in stereolithography

Setareh Zakeri*, Minnamari Vippola, Erkki Levänen

Materials Science and Environmental Engineering, Faculty of Engineering and Natural Sciences, Tampere University (TAU), Tampere, Finland

A B S T R A C T

In recent years, there have been rapid advances in our understanding of ceramic stereolithography (CSL) as a precise and high-resolution additive manufacturing (AM) technique to fabricate complex ceramic parts. This review highlights the theoretical background and engineering capabilities of CSL with an emphasis on photopolymerization of ceramic resins. We present certain constraints and characteristics designed to achieve optimal printability and photo-curability goals in ceramic resins and discuss in details about the parameters that can affect these properties. We then describe the current market status of CSL as well as its remaining challenges and promising future directions.

1. Introduction

Ceramic materials are used in a wide range of applications owing to their outstanding properties, such as high hardness and strength, good high-temperature performance, excellent thermal shock resistance, and high chemical stability in harsh conditions [1,2]. However, it has always been a challenge to shape and process ceramic parts because of their inherent hardness and brittleness [2]. Conventional shaping methods, such as dry pressing, tape casting, slip casting, gel casting, and injection molding, are not capable of producing highly complex structures with detailed features [3]. Moreover, most of these shaping methods require molds, and the sintered parts typically require mechanical processing [1].

In contrast, additive manufacturing (AM) offers new routes to overcome the aforementioned disadvantages of the conventional methods, and it fabricates highly complex ceramic components [4]. AM, also known as three-dimensional (3D) printing, is a rapid prototyping technology for manufacturing complex 3D parts without molds in a short time [5,6]. According to ASTM/ISO standardization, AM technologies can be categorized into seven distinct classes, including selective laser melting, selective laser sintering, fused deposition modeling, laminated object manufacturing, direct ink writing, and stereolithography (SL) [7]. These techniques use the same process to construct components: printing successive two-dimensional (2D) layers of the starting material on top of each other until the entire 3D part is built [8].

Among these potential techniques, SL fabricates high-quality parts with higher resolution and smoother surface finish [9,10]. In 1986, Charles Hull invented SL, which produces 3D plastic parts by selectively irradiating and solidifying (photopolymerizing) layers of liquid resins made of photocurable monomers [7]. In 1994, Griffith et al. combined SL and ceramic manufacturing processes to build 3D ceramic parts [1]. This adapted version of SL for the fabrication of ceramic parts, rather than plastic parts, is known as ceramic stereolithography (CSL). In CSL, conventional raw resins are loaded with ceramic powders acting as fillers, and the ceramic-loaded resins are typically called ceramic resins. The presence of ceramic fillers increases the resin viscosity and reduces resolution owing to light scattering. Although the challenges of CSL and SL are different, the concept of photopolymerization is the same for both raw and ceramic resins [11].

This review paper aims to provide fundamental knowledge and practical understanding of CSL. As both SL and CSL have the same principle of operation, this review first focuses on the basics of SL and later CSL and their related issues.

2. Stereolithography

All AM techniques are based on the same basic principle: a computer-aided design (CAD) file of the part to be manufactured must be first sliced into a series of 2D cross-sectional layers, and subsequently, a 3D solid part can be built by fabricating those 2D sliced layers one by one. In SL, the thin 2D layers of a photocurable resin consisting of photopolymerizable monomers, such as acrylates or/and epoxides, are successively exposed to laser irradiation. Consequently, these liquid layers become solidified on top of each other until a 3D part is entirely built [12]. The laser beam supplies the energy required to induce the photopolymerization process, bond many small monomers, and form a highly cross-linked polymer [13].

* Corresponding author.
E-mail address: setareh.zakeri@tuni.fi (S. Zakeri).

https://doi.org/10.1016/j.addma.2020.101177
Received 29 October 2019; Received in revised form 6 February 2020; Accepted 13 March 2020
Available online 19 May 2020

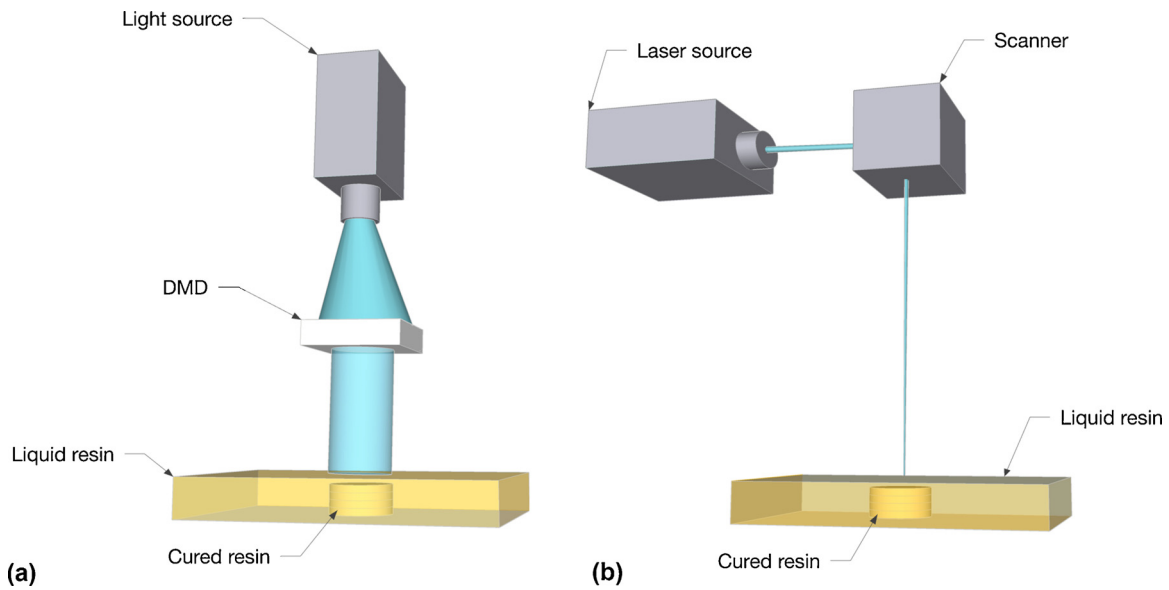

Fig. 1. Schematic design of two basic approaches for stereolithographic systems: PSL (a) and SSL (b).

As shown in Fig. 1, SL can be categorized into two classes based on the mechanism of applying UV light to the resin layer and solidifying it: projection-based stereolithography (PSL) and scanning-based stereolithography (SSL).

The PSL approach cures the entire layer at once by using a light mask through which a flood lamp illuminates the resin surface (Fig. 1 (a)). The light mask in this system is dynamically generated by a digital micromirror device (DMD), which produces an image of each layer. PSL is appropriate for higher resolution printing of small parts due to the limited size of the patterned laser light. Moreover, PSL requires less printing time because each layer is printed in a single shot. In contrast, the SSL approach uses a laser scanner to cure each layer (Fig. 1(b)). A dynamic mirror system is used to focus and direct the laser beam over the resin surface to polymerize a set of elementary volumes known as strands. In general, SSL is suitable for large size printing, however, at the cost of resolution [13–15].

2.1. Configuration of stereolithography apparatus

Fig. 2 shows a schematic design of a scanning-based stereolithography apparatus (SLA).

In general, SLA consists of five core components: vat, recoater, platform, optics, and control systems. In SL, the starting material is in the form of a liquid photocurable resin contained inside the vat, which is usually integrated with an automated refilling pump and a level adjustment device. Liquid resins used in SLA can be relatively viscous; therefore, the resin surface cannot become flat owing to gravity alone. Hence, the recoater blade is typically used to distribute the resin and flatten its surface uniformly. The platform system is composed of a building platform on which the part is fabricated, and an elevator, which raises and lowers the building platform [7,16]. The optics system consists of a laser source (Diode, He-Cd, Argon), an acoustic optical modulator to switch the laser beam on and off rapidly, a Z-focus lens to maintain the laser in focus on the resin surface, and two inertia galvanometers to scan the laser beam across the resin surface. The control system comprises three components: (1) a process controller to check the sequence of machine operations, (2) a beam controller to convert the operation descriptions into actions for adjusting the scanning speed and focus depth, and (3) an environment controller to adjust the temperature and humidity of the chamber that contains the vat [7,12].

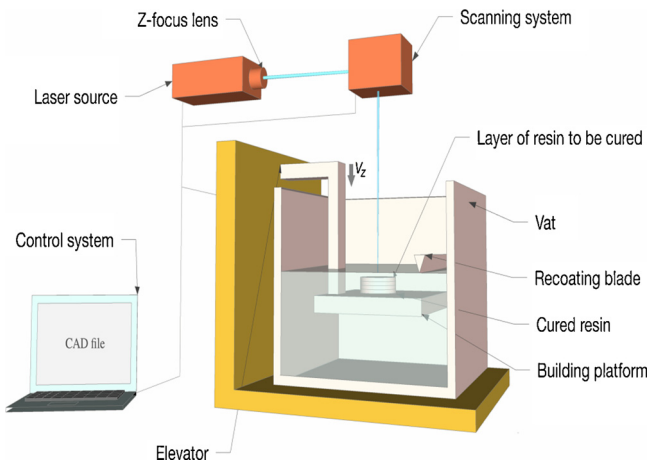

Fig. 2. Schematic design of a typical scanning-based SLA (top-down orientation).

2.2. Orientation approaches of stereolithography apparatus

SLA may have two orientation approaches, i.e., top-down and bottom-up, depending on the light projection technology used in the device. In the top-down approach, the laser source is positioned above the vat, and parts are fabricated facing upward (Fig. 2). The building platform is immersed inside the vat and positioned immediately below the resin surface. Only a thin layer of resin, with a specific thickness, is exposed to the laser source from above. Once a layer is cured, the building platform moves downward along the *Z*-axis by one-layer thickness to spread a fresh resin layer on top of the previously cured layer [17–20].

This set-up suffers from several problems. The downward movement of the platform disturbs the equilibrium of the resin level, consuming extra time for the recovery of the equilibrium state and reducing the efficiency of the entire procedure. Moreover, it is difficult to control the layer thickness in this set-up because only gravity is involved in leveling the resin surface after the deposition of a fresh layer on top of the previously cured layer. The resin surface can be leveled by using the recoater blade. However, this process is time-consuming. Hence, low-viscosity resins are recommended for use in this set-up [21,13,22]. Surface tension can also be a problem when leveling the resin surface around the already printed part. Furthermore, the fresh resin layer is

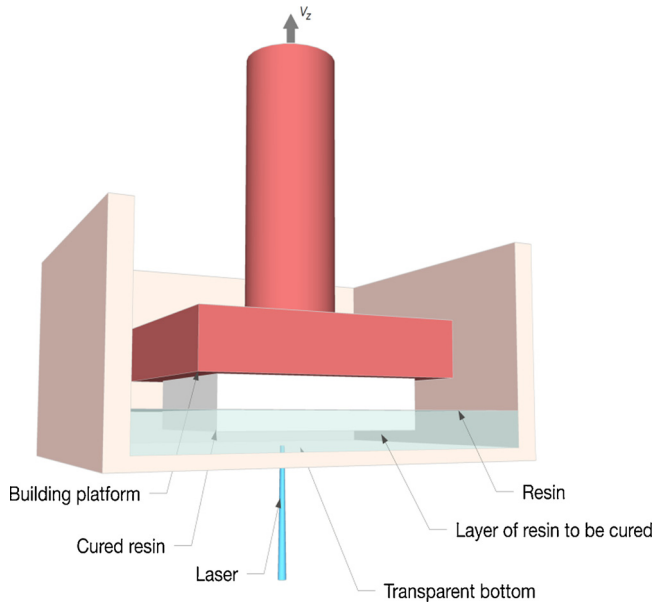

Fig. 3. The bottom-up orientation approach of a typical scanning-based SLA.

always in contact with the oxygen in the air, which inhibits the photopolymerization of certain monomers, resulting in incomplete curing and surface tackiness. Moreover, this approach requires a large vat and more resin [23,24].

The bottom-up approach provides excellent potential to overcome the problems encountered in the above set-up. Unlike in the top-down approach, photopolymerization is performed by an irradiation source beneath the vat (Fig. 3).

This orientation requires a vat with a transparent and non-sticky bottom for the gentle detachment of each cured layer [22,19,25]. In this set-up, the vat is shallow, and less material is required. The building platform is positioned inside the vat against the transparent bottom, leaving only a small gap with one-layer thickness. Once a layer is exposed to UV light from beneath, the cured layer is sandwiched between the vat bottom and the previously cured layer. The building platform rises each time a layer is cured to peel off the cured layer and allow fresh resin to flow in between the vat bottom and the last cured layer. Therefore, the fresh resin to be cured is less in contact with oxygen, resulting in a higher photopolymerization rate. The part height is not limited to the vat depth as the part is built facing downward. The layer thickness can be precisely achieved because it is accurately controlled by the elevator and not by the resin fluid properties. Thus, this technique offers higher vertical resolution and better surface quality [26,25,27,17]. The major drawback of this configuration is the cured layer adhesion to the vat bottom. Suitable coatings, such as Teflon and silicone films, can be applied on the transparent vat bottom to reduce the attachment force, resulting in successful detachment of the part from the vat bottom [13,28].

2.3. Fundamental parameters of stereolithography apparatus

The fundamental parameters of the SL process can be divided into two groups: (1) technical parameters, which can be adjusted using the SLA, such as laser power, laser scanning velocity, layer thickness, and hatch spacing, and (2) photosensitive parameters, which are the intrinsic properties of the resin, such as penetration depth and critical energy dose. These parameters have a substantial effect on the geometrical accuracy of the manufactured parts [29,30].

Conventional photocurable resin is considered a relatively transparent medium, allowing UV light to pass through it. The laser intensity distribution through this medium runs the photopolymerization process and determines the cured areas. The laser beam used in SL is Gaussian, which indicates that its intensity decreases from the beam center according to the Gaussian law. The Gaussian beam propagates along the Z-axis with a symmetry axis coinciding with the Z-axis. Fig. 4(a) shows the Gaussian distribution of light exposure, which is defined as the laser source radiant energy per surface unit [31]. Once the Gaussian laser beam scans a straight line at a constant velocity over the resin surface, a parabolic cylinder is solidified, which is often referred to as a strand (Fig. 4(b)). The curing profile reflects the intensity distribution of the incident beam. Each strand has a specific depth and width known as the curing depth (C_d) and curing width (C_w), respectively [32,30]. These two parameters have a significant impact on the vertical and lateral resolutions [33,34].

In modeling the photocuring behavior, it is assumed that photocurable resins obey the Beer–Lambert law of exponential absorption. According to this law and as also depicted in Fig. 4 (b), the exposed light has its maximum energy value (E_{max}) at the resin surface (dark blue), and it exponentially attenuates as light penetrates through the resin absorbing medium (light blue). Therefore, it can be concluded that the UV light penetration through the resin is limited because of its dispersion and absorption. The extent of photopolymerization increases with UV light illumination until the resin reaches the gel point, at which it is converted from the liquid-state to solid-state. C_d is defined as the depth at which light energy is sufficient to bring the resin to the gel point. The light energy at C_d is called critical energy (E_c) and is required to initiate photopolymerization. As shown in Fig. 4(b), the resin reaches the gel point if the light energy is higher than E_c; otherwise, it remains a liquid [32,35]. C_d is calculated using Jacob's version of the Beer–Lambert law:

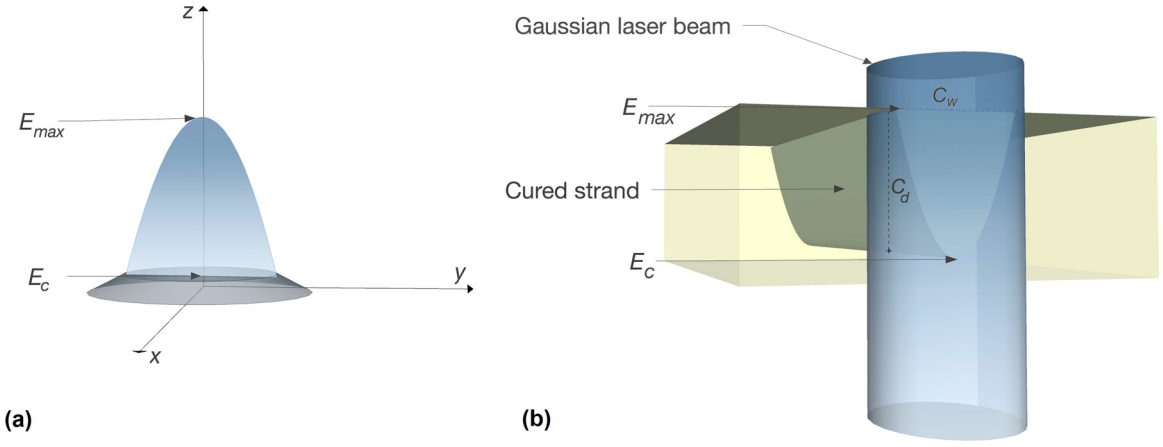

Fig. 4. The Gaussian distribution of the (a), a cured strand and light attenuation in a photocurable resin (b) (Inspired by [11]).

$$C_d = D_p \ln\left(\frac{E_{\max}}{E_c}\right) \quad (1)$$

where D_p is the penetration depth at which the beam intensity is reduced to $1/e^2$ (37%) of its value at the resin surface.

The photocuring behavior is characterized by plotting C_d (μm) versus $ln(E_{max})$ (J/cm^2) using a semi-log plot. The result is a line known as the working curve, from which D_p and E_c can be calculated. D_p is the slope of the line, and E_c is its intercept with the X-axis.

Both D_p and E_c are purely resin parameters and are independent of the exposure. Therefore, both the slope and intercept of the working curve are independent of the technical parameters, such as laser power, laser spot size, and laser scanning speed [32,36].

In SLA systems, E_{max} can be controlled using two adjustable parameters: light power and scanning speed, which determines the light exposure time. E_{max} is derived using the following equation:

$$E_{\max} = \sqrt{\frac{2}{\pi}} \frac{P}{w_0 v_s} \quad (2)$$

In this equation, P is the laser power, w_0 is the beam radius, and v_s is the scanning speed. As indicated by Eq. (2), E_{max} is proportional to the laser power and inversely proportional to the product of the beam radius and the scanning speed. By combining Eqs. (1) and (2), it can be elucidated that C_d can be controlled by changing the level of radiation applied to the resin surface [13,32].

In addition to C_d, C_w is a key parameter in the SL process, and it strongly affects the lateral resolution. As shown in Fig. 4 (b), the maximum cured width occurs at the resin surface where the width of the parabolic cylinder is largest. This parameter can be calculated using the following equation:

$$C_w = w_0 \sqrt{\frac{2C_d}{D_p}} \quad (3)$$

As indicated by Eq. (3), C_w is directly proportional to the laser spot size and the square root of the ratio of C_d to D_p. Thus, strands with greater C_d are also wider. However, the relationship between them is not linear. Notably, when w_0 and C_d are maintained constant, C_w depends only on D_p. This is useful to remember when the resin must be changed [32].

In addition to the aforementioned parameters, some other important parameters affect the resolution of SL, such as layer thickness, hatch spacing, and hatch overcure (Fig. 5). Layer thickness is one of the most important working parameters and is the depth of a layer solidified at the same elevation. This user-definable parameter is the thickness of the 2D sliced layers of the part CAD model. In the building process, the layer thickness is controlled by lowering/raising the building platform inside the resin vat for a predetermined, shallow thickness [30,38,37].

The hatch strands are located in the region within a layer sandwiched between the additional part layers [13]. The distance between the two adjacent hatch strands is known as “hatch spacing.” If hatch spacing is very small, the solidified strands will overlap, resulting in a solid layer. In contrast, when hatch spacing is large, the liquid resin will be trapped inside the part, and it must be solidified in the following post-curing step [39,30]. Overcure is the depth through which each strand slightly penetrates the lower adjacent layer, and it increases the curing of that layer. Overcure is the main reason that keeps the individual layers connected together to construct a complete 3D part. To assist the bonding of the printed layers, C_d should be equal to the layer thickness plus a certain amount of overcuring. Typically, overcure is suggested to be estimated as approximately 10%–35% of the layer thickness to avoid problems such as delamination and print-through.

3. Fundamentals of photocurable resins

3.1. Photopolymerization and photocrosslinking

Polymerization is defined as the generation of macromolecules with longer chain length through the continuous addition of monomers/oligomers with shorter chain length. This addition can be induced by several stimuli, such as heat, electron beam, and light. The photo-induced polymerization process is a chain reaction in which one photon yields initiating species and induces the incorporation of thousands of monomer/oligomer units. This process is called photopolymerization, in which monomers in the form of a liquid are converted into a solid polymer in a few seconds [40–42]. Photopolymerization depends on not only light quantity but also light quality (wavelength). The wavelength range used in photopolymerization includes both UV (200–400 nm) and visible (400–700 nm) light. Most commonly, the wavelength required for the photopolymerization of resins is in the blue region. In some rare cases, infrared light (700–1000 nm) has also been used [42,43]. If monomers and oligomers are multifunctional, which indicates that they contain at least two functional groups in their structure, photopolymerization shows a complex behavior. In addition to the

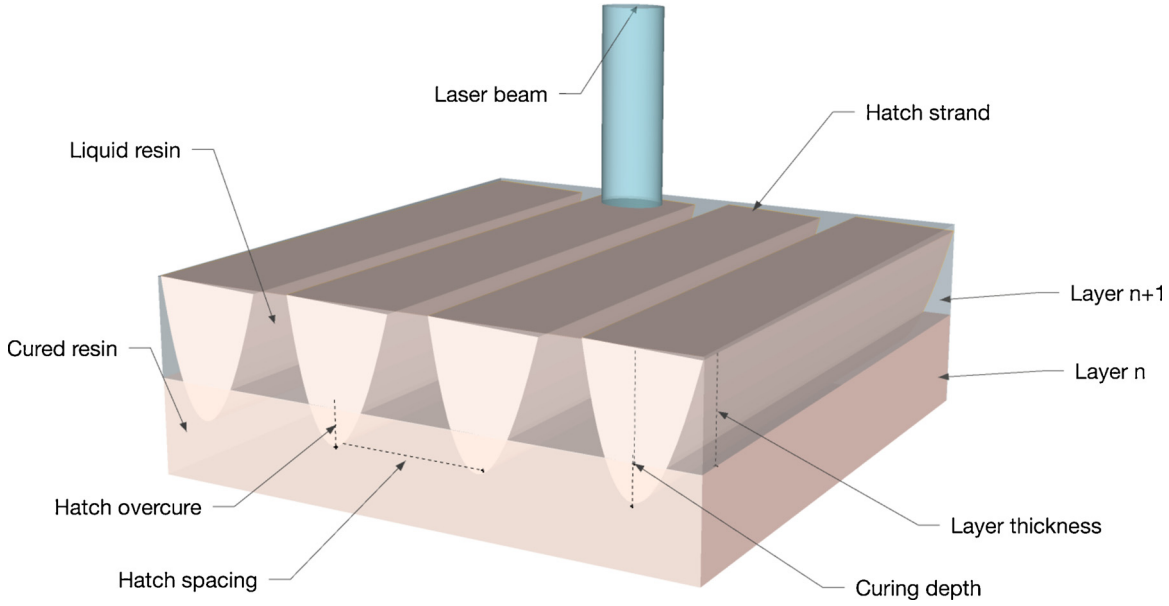

Fig. 5. Schematic view of some of the working parameters of SLA: Layer thickness, hatch spacing, hatch overcure and border overcure (Inspired by [30]).

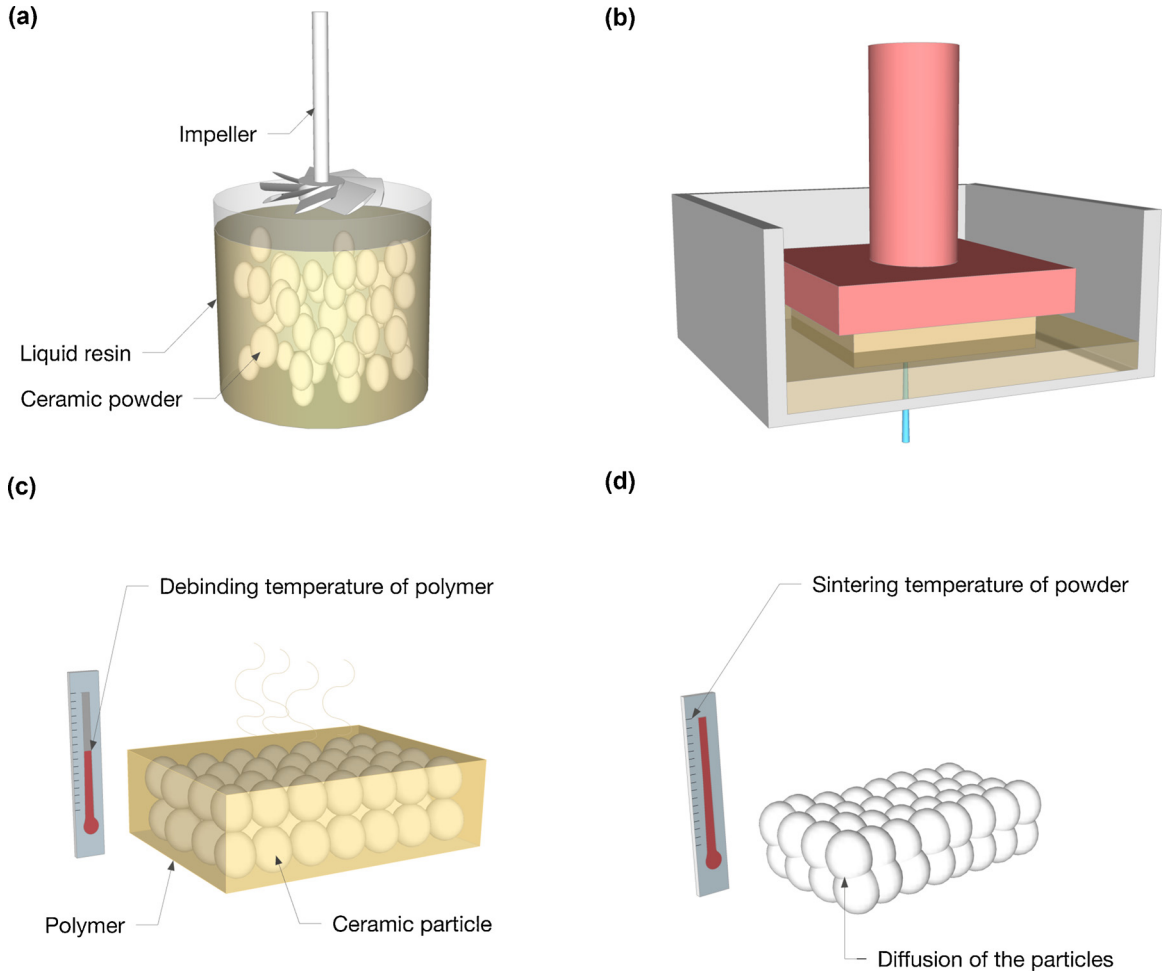

Fig. 6. The flowchart of the steps in CSL: preparing a suitable photocurable ceramic suspension by mixing ceramic powder and liquid resin (a), actual building of ceramic part (b), debinding and removing the polymer (c) and sintering the ceramic green body (d).

formation of a linear chain of monomers, a cross-link is formed between two linear macromolecular chains, forming a 3D network structure. This process is known as photocrosslinking, and it does not occur in the polymerization of monofunctional monomers [13,44,42].

Photopolymerization requires monomers/oligomers, which polymerize to form highly cross-linked polymer structures, and photoinitiators (PIs), which generate reactive initiating species upon UV exposure [45,13]. Hence, conventional raw resins used in SL consist of PIs (~5 wt.%), monomers (~25 wt.%), and oligomers (~70 wt.%). Additional components, such as inert dyes, dispersion agents, inhibitors, fillers, and plasticizers, can be added into the resin in low concentrations to optimize the properties of the resin [42].

3.1.1. Photoinitiator

Most monomers/oligomers do not generate reactive species to initiate photopolymerization per se. Therefore, low-molecular-weight organic PIs are used in resins to generate reactive species to attack the functional groups of monomers/oligomers. Once the functional group is decomposed, each reactive double bond C=C can form a new bond with another carbon atom from a different monomer molecule. When the strong covalent bonds replace the weak van der Waals interactions between adjacent molecules, the liquid resin transforms into a solid structure with different bulk properties [47,13,46].

Free-radical PIs form free radicals after the absorption of the incident UV light, which immediately attack the double bonds of specific monomers, such as acrylates and methacrylates [13,48]. In contrast to free-radical PIs, cationic PIs produce acids when exposed to light. The generated acids readily react with a bond in specific monomers, such as vinyl ethers and epoxides, and induce polymerization [14].

3.1.2. Oligomers

Oligomers (prepolymers/macromonomers) are molecules with intermediate molecular weight possessing a larger chain structure consisting of a few monomer units. Oligomer is the main component of raw resins, and it determines the final desirable physical and chemical properties of the cured film. However, it is rarely used in concentrated ceramic resins as it is typically in the form of a viscous liquid, which makes it difficult to deal with [46,42].

3.1.3. Monomers

In raw resins, monomers are used as reactive diluents, and are mainly added to reduce the viscosity of oligomer and control the properties of the cured film [42,49]. In ceramic resins, they are the major component of the photocurable liquid resin due to their low viscosity. They can be categorized into two different groups depending on the type of reaction required to polymerize them.

Monomers based on free-radical reactions require free radicals to initiate polymerization. Therefore, only free-radical PIs can induce the photopolymerization of this type of monomers. Once a monomer accepts a free radical from PIs, it transfers that radical to another monomer to form a polymer. Acrylates and methacrylates are the most widely used monomers for free-radical photopolymerization [49].

Monomers based on cationic reactions require only cationic PIs to initiate photopolymerization. Several classes of monomers, such as

Fig. 7. Ceramic parts manufactured by using CeraFab 7500 at Tampere University (Credit goes to Teemu Vastamäki and Jorma Vihinen for the fabrication of these parts).

epoxides, vinyl ethers, propenyl ethers, siloxanes, cyclic acetals, and furfural, polymerize under the cationic mechanism. Epoxide is the most famous monomer in this class [50].

4. Ceramic stereolithography

The addition of fillers, such as hollow glasses and ceramic microspheres, into a raw resin was introduced by Fan [51]. This idea was initially proposed to reduce the typically large C_d of raw resins. Fan proposed that the dispersed filler particles in the resin can deflect the incoming radiation, resulting in a decrease in C_d and an increase in resin opacity. The novelty of this work was later used in CSL, which is a promising technology for the fabrication of advanced ceramic parts with complex geometries because of its high resolution [52]. CSL has significantly advanced during the last two decades, making it possible to produce ceramic parts with demanding end-use applications rather than building only prototypes [53].

As shown in Fig. 6, the CSL process consists of the following main steps: preparing a suitable photocurable ceramic suspension, the building of the ceramic part, debinding, and sintering. The preparation of photocurable ceramic resins requires the homogenous dispersion of ceramic particles in conventional raw resin. The addition of ceramic powders significantly increases the resin viscosity; therefore, processing of ceramic resins becomes more difficult compared with that of raw resins [54,55]. The building of ceramic parts has similar steps as those in SL. During the photopolymerization of ceramic resin, monomers/oligomers act as a binder and constitute a matrix around the ceramic particles by bonding them together. This matrix confers sufficient cohesion to the fabricated green body, which is a composite part consisting of polymer and ceramic. In general, the composite green body is stiffer and stronger than the pure polymeric part [56,19].

In this technique, obtaining a pure ceramic part requires that the composite green body be subjected to appropriate thermal treatments. First, the organic phase (binder) should be removed through a specific treatment step (debinding). Subsequently, a second thermal treatment (sintering) must be applied at higher temperatures to achieve acceptable mechanical properties. The resin thermal analysis should be performed before any thermal treatment. This step ensures that appropriate thermal treatment is selected for debinding, in which the green body is heated at slow rates, usually up to 500 °C. Slow heating rates avoid typically high shrinkage rate, prevent fast gas formation, and maintain even temperature distribution during debinding. Therefore, the final properties of the end-product are not downgraded. Debinding is followed by sintering, in which the ceramic part should undergo heating treatment from 500 °C to high temperatures depending on the sintering temperature of the ceramic powder. Sintering eliminates the voids in the ceramic part by shrinkage and thus increases its density [52].

4.1. Advanced ceramic materials used in ceramic stereolithography

The following requirements should be satisfied for the utilization of ceramic materials in SL [57,58,19,59]:

1 The ceramic powder should present a small variation of refractive index (RI) with one of the raw resins. In the UV wavelength range, ceramic materials have RI ranging from 1.56 (silica) to 2.6 (silicon carbide), and most monomers have RI of approximately 1.5. Therefore, it is recommended to utilize ceramic powders having low or medium RI, such as silica and alumina.
2 The ceramic powder should not strongly absorb light in the UV wavelength range because UV light should penetrate through the ceramic resin for the photopolymerization process. Thus, it is challenging in CSL to employ ceramic materials, such as titania and silicon carbide, which are highly absorbing and opaque at UV wavelengths.
3 The ceramic powder should have a median particle size (d_{50}) smaller than the layer thickness, which is typically in the range of 25 μm to 100 μm. This requirement improves the vertical resolution of the fabricated part. In general, the suitable particle size is suggested to be between 0.05 μm and 10 μm.

Despite the constraints in the material development, various ceramic materials, such as alumina (Al_2O_3), zirconia (ZrO_2), silica (SiO_2), hydroxyapatite (HA), zirconate titanate oxides (PZT), and silicon nitride (Si_3N_4), have been used in CSL so far [13]. Among these ceramic materials, more extensive research has been conducted on the preparation of alumina [6,60,4], zirconia [61,1,62], and silica [63–65] resins. Fig. 7 shows some of the complex 3D alumina and zirconia parts fabricated using CeraFab 7500 from Lithoz GmbH at Tampere University.

4.2. Light attenuation in ceramic resins

Conventional raw resins are homogeneous and relatively transparent to the incident laser beam used for photopolymerization. The C_d of such resins is relatively large because light attenuation in such a medium relies solely on absorption, which occurs owing to the absorbing agents present, such as PIs and inert dyes. The absorption process is dependent on the concentration and extinction coefficients of the absorbing agents [66,67].

Homogeneous raw resins become heterogeneous and more complex when small ceramic particles are mixed with them [66,57]. The submicronic and micronic ceramic particles suspended in photocurable resins significantly disrupt the photopolymerization process because of light scattering. Scattering is an optical phenomenon in which the direction of light changes owing to the presence of non-uniformities in the medium. The main difference between ceramic resins and conventional resins is the scattering of the forward beam, which deviates some of the UV radiation from the forward direction [31,68,11].

As shown in Fig. 8, a photon is scattered by a suspended particle in a ceramic resin when it hits the particle. Light scattering occurs at interfaces with different RIs, and the scattering coefficient can quantify it. This parameter, defining the efficiency of particles to scatter light, is dependent on several variables, such as the median particle size, the number of particles, and RI contrast between the particles and medium. Ceramic powders with smaller particle sizes have more surface area and interfaces. Thus, more scattering occurs in ceramic resins composed of fine particles. In contrast, larger particles transmit more light. It is evident that, by increasing the number of particles per unit volume, more scattering events occur in the medium. Moreover, scattering

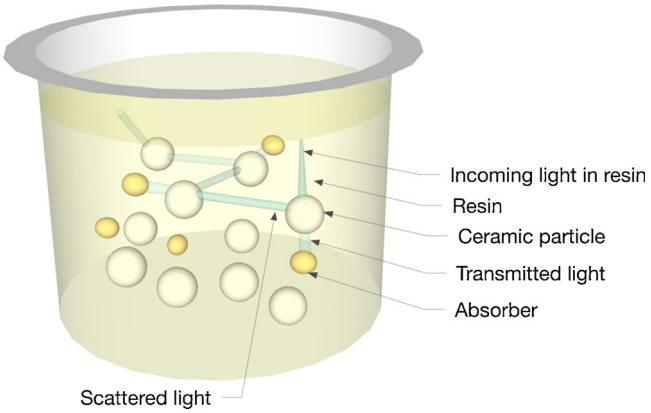

Fig. 8. Simple view of the scattered light (only in one direction) and transmitted light as a light ray hits a suspended ceramic particle in liquid resin.

increases when the RI contrast is increased, indicating that particles with higher RI scatter light into larger angles of deflection [69].

The scattered light is not lost from the exposed medium, unlike the absorbed light. It only changes its direction and contributes to other directions [38]. Therefore, both light scattering and absorption attenuate the energy intensity of the light traversing the resin medium with dispersed solid particles [68,70,32]. Tomeckova and Halloran [67] proposed a predictive model that describes the light attenuation in ceramic resins. According to their work, the attenuation coefficient ($1/D_p$), which is the inverse of resin sensitivity or penetration depth, can be modeled by the following equation:

$$\frac{1}{D_p} = S + A - A\phi \tag{4}$$

where S describes the scattering effect of ceramic particles, A represents the light absorption by PIs and inert dyes, and ϕ represents the volume fraction of ceramic powder in the resin.

The term S is related to the inverse of the scattering length (l^*), which is defined as the distance passed by a photon before its propagation direction becomes randomized. A small scattering length corresponds to a considerable degree of scattering, whereas a large scattering length indicates a minimal degree of scattering. A ceramic suspension with a large scattering length is expected to have a cured profile, which is similar to that of conventional SL resins [68]. Thus far, there has been no simple closed-form expression for the scattering length in highly loaded suspensions. However, it has been experimentally determined that S increases as the ceramic volume fraction increases up to its maximum amount ϕ_{max}.

Moreover, the term A is related to the properties of PIs and inert dyes as given by the following equation:

$$A = \varepsilon_P c_P + \varepsilon_D c_D \tag{5}$$

As indicated by Eq. (5), the light absorption by PIs can be quantified by $\varepsilon_P c_P$, which is simply the product of the concentration (c_P) and extinction coefficient (ε_P) of the PI. The light absorption by inert dyes can be quantified by the product of the concentration (c_D) and extinction coefficient (ε_D) of the dye [71].

Therefore, Eq. (4) can be rewritten as [67]

$$\frac{1}{D_p} = S + (1-\phi)(\varepsilon_P c_P + \varepsilon_D c_D) \tag{6}$$

As indicated by Eq. (6), the ceramic powder dispersed in resin plays two significant roles: it attenuates UV light by scattering through the term S, and it reduces the photopolymerization rate (conversion) by diluting the resin through the term $(1-\phi)$ [71].

4.3. Effect of scattering on curing depth and curing width

When the laser beam with an ideal Gaussian lateral intensity distribution penetrates a raw resin, in which no scattering occurs, the curing profile reflects the intensity distribution of the incident beam. Therefore, the curing profile has a narrow bullet-shaped structure, whose depth is typically larger than its width (Fig. 9(a)) [35,29].

In contrast, the curing profile of ceramic resins is significantly different from the lateral intensity distribution of the Gaussian beam [35]. The curing profile of a ceramic resin is shallower than that of a raw resin because of light scattering. Although a ceramic resin might be composed of UV-transparent ceramic powder, the radiation scattering process generates high turbidity in the medium, which reduces the C_d [72]. Moreover, light scattering delivers more radiation in sideways directions and enlarges C_w. Therefore, unlike raw resins with a narrow curing profile, ceramic resins exhibit profile broadening, which degrades the feature resolution. In ceramic resins, the curing profile is typically shallower and broader, and it has a mushroom-shaped structure (Fig. 9(b)). Therefore, it can be concluded that the presence of solid particles in ceramic resins reduces the printing accuracy owing to light scattering [73,52,14]. It is necessary to control C_d and C_w to obtain dimensional accuracy because both are essential parameters to be considered for printing detailed structures.

As thoroughly explained in Section 2.3, the C_d of raw resins can be expressed by Eq. (1). However, ceramic resins consisting of a high volume fraction of ceramic powder do not obey this equation [38] because light attenuation in ceramic resins is also controlled by scattering rather than merely absorption [73]. The C_d of such resins can be expressed by the following equation [57]:

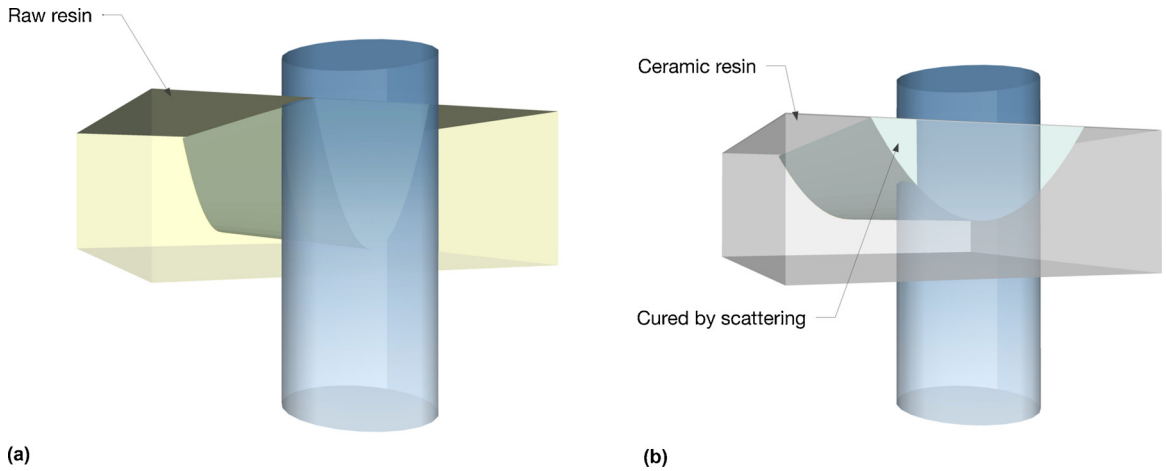

Fig. 9. The curing profile of a photocurable raw resin (a) and a photocurable ceramic resin (b) once laser beam scans a straight line at constant velocity.

$$C_d = \frac{2}{3} \times \frac{d}{\phi\beta\Delta n^2}(\ln \frac{E_{\max}}{E_c}) \quad (7)$$

where d is the mean particle size of the powder, ϕ is the volume fraction of the powder, β includes the particle size and laser wavelength, and Δn is the RI contrast, which is the difference between the RIs of the suspended ceramic particles (n_c) and the photocurable matrix (n_0).

By comparing Eqs. (1) and (7), it can be concluded that D_p can be expressed by Eq. (8), which includes the scattering effect [74]:

$$D_p = \frac{2}{3} \times \frac{d}{\phi . Q} \quad (8)$$

where Q is a factor representing the capability of matter to diffuse radiation and is given by the following equation:

$$Q = \frac{h}{\lambda} . \Delta n^2 \quad (9)$$

where h is the interparticle distance, and λ is the wavelength of the irradiation.

By combining Eqs. (8) and (9), it can be deduced that D_p or resin sensitivity is affected by the properties of the ceramic resin, including the solid loading of ceramic powder, the size of the suspended particles, and the RI of both powder and liquid resin. D_p depends on the properties of the ceramic resin because the light scattering phenomenon is affected by the same properties. If D_p is large, then small C_d can be achieved by decreasing E_{max}. In contrast, when D_p is small, small C_d can be achieved by increasing E_{max} [71].

Moreover, C_w in the horizontal platform can be calculated using the following equation:

$$C_w = w_0 \sqrt{\frac{2C_d}{D_p}} \quad (10)$$

As indicated by Eq. (10), C_w is proportional to the beam spot size and is always larger than the laser beam diameter ($2w_0$), suggesting a significant influence of lateral scattering. Furthermore, C_w always increases upon increasing C_d [75].

It is evident from Eqs. (7) and (10) that both C_d and C_w are significantly affected by the working parameters of the SLA and the parameters related to the ceramic powder, such as its volume fraction, RI, and mean particle size. For instance, more UV light is scattered when Δn is large. Owing to this strong scattering, both D_p and C_d are reduced. Moreover, more scattering events cause more resin around the laser beam to become cured. Thus, C_w increases, and consequently, the lateral resolution is reduced. Therefore, choosing an appropriate liquid resin for a specific ceramic powder to reduce Δn is a crucial step for the fabrication of detailed structures [14].

4.4. Suitable photocurable ceramic resins

An essential step in CSL is to prepare a suitable ceramic resin, in which a fine ceramic powder should be mixed with a monomer-containing solution. This system often requires the addition of a dispersant to maintain resin stability and prevent agglomerations. In general, current photocurable ceramic resins can be divided into two groups: aqueous (acrylamide-based) and non-aqueous (acrylate- and epoxy-based) resins [57,52].

In 1994, Griffith et al. [59] introduced the first aqueous photocurable suspension used in CSL. The prepared aqueous acrylamide-based solutions had low RI (1.38–1.44). Thus, the Δn was large, resulting in a small C_d. Therefore, the choice of ceramic powders to be mixed with the aqueous resins is limited. Although this group of ceramic resins has several advantages, such as low viscosity, freedom from volatile organic compound emissions, and the ease of dispersing oxide ceramic powders, it has one main disadvantage related to the low strength of the as-gelled green body. Moreover, a large amount of water present in the suspension introduces several problems, including cracking and drying of the green body [38]. This group of ceramic resins has not been widely used and studied in CSL owing to these problems [76].

In contrast, non-aqueous ceramic resins have the advantage of providing higher strength for the cured green body, compared with aqueous ceramic resins. Therefore, many researchers have investigated this group of ceramic resins [77]. The acrylate- and epoxy-based resins typically have larger RI (1.47–1.55) than aqueous resins, which is very beneficial because only a small increase in the RI of the monomer solution can dramatically increase the C_d. Thus, even a low E_{max} is sufficient to cure a given C_d, resulting in faster operation time. Non-aqueous ceramic resins are favorable for the processing of non-oxide ceramics because of the problems faced owing to the hydrolysis and oxidation of non-oxide particle surfaces in aqueous resins [38]. However, this group of photocurable ceramic suspensions has the limitation of having higher viscosities than those of aqueous suspensions when the same volume fraction of ceramic powder is used in the resin formulations [77].

It has been proven that the same formulation cannot be used for the preparation of other ceramic resins with various ceramic powders or monomer solutions. Hence, it is recommended that, for each ceramic type or compound, a specific formulation should be individually examined [72]. Thus far, numerous studies related to the development of ceramic resins have been conducted. Some of these studies are summarized in Table 1, which includes only some of their partial or final successful results. Such developmental research is crucial as the final quality of the fabricated part is strongly dependent on controlling the rheological and photocuring characteristics of the ceramic resin. In general, a photocurable ceramic resin should satisfy a few requirements to be printable including having high solid loading, low viscosity, and adequate C_d.

4.4.1. High solid loading

In powder processing and consolidation of ceramics, the aim is to achieve high green density to produce ceramic parts with excellent dimensional and structural integrity. For the fabrication of high-quality and dense ceramic parts, the ceramic powder content or loading in green bodies should be as high as possible [54,108]. This requirement should also be satisfied in CSL because the as-gelled green bodies with low ceramic loading suffer from excessive shrinkage and delamination during the debinding and sintering steps [48]. Hence, typically, 50 vol. % ceramic powder is sufficient, but even higher loadings are desired. It is highly recommended to reduce the organic concentration of the suspension because high solid loading improves the final properties of the end-product by [54]:

- minimizing porosity, which limits the strength of the part.
- accelerating the debinding process and reducing the risk of part disruption.
- reducing sintering shrinkage and avoiding deformation and cracking.
- providing dense and homogeneous sintered ceramic parts.

The sintered ceramic part can have a density up to 99.9% of its theoretical density if the prepared suspension has sufficiently high solid loading and contains no air bubbles, and laminar defects are avoided while building and processing the part [54].

4.4.2. Low viscosity

Ceramic resins used in CSL should be highly mobile to produce ceramic parts with complex geometries within a reasonable processing time [48]. In other words, the resin viscosity should be relatively low, preferably with no pronounced yield point. This condition is required to facilitate the recoating and self-leveling of the resin [73]. Ceramic resins should be as fluid as conventional raw resins, with viscosities less than 3000 mPa·s, to conduct the CSL process in an SL resin vat [72]. This situation corresponds to a ceramic loading of less than 50 vol.%.

Table 1
The main properties of some of the suitable ceramic resins for the CSL process and the energy and wavelength of the laser.

Powder	Particle size (μm)	Resin composition	Solid loading (vol.%)	Viscosity (*Pa. s*)	C_d/D_p (μm)	E_{max}/E_c (mJ/cm^2)	Laser wavelength (nm)	Reference
Al_2O_3	0.2	HDDA[a] + PPTTA[a] + PPG400[b]	50	3.98 at 100 s^{-1}	D_p: 65.2	E_c: 3.84	405	[78]
Al_2O_3	4.4	Acrylates	50	-	D_p: 68	E_c: 4.8	351-364	[74]
Al_2O_3	0.4	HDDA + 2-HEA[a] + TMPTA[a]	45	1.62 at 30 s^{-1}	-	-	405	[79]
Al_2O_3	0.4-0.7	HDDA + PPTTA	56	-	D_p: 56.36	E_c: 4.6	405	[80]
Al_2O_3	10.34	Commercial resin	60	15.4 at 200 s^{-1}	-	-	-	[4]
Al_2O_3	0.5	HDDA + TMPTA	40	≈ 3 at 45 s^{-1}	-	-	364	[81]
Al_2O_3	0.138	HDDA + Acrylated monomer	60	3.1	-	-	-	[82]
Al_2O_3	0.5	HDDA + PPTTA	50	3 at 100 s^{-1}	-	-	355	[83]
Al_2O_3	0.4	HDDA	40	< 3 at 30 s^{-1}	D_p: 46.61	E_c: 30.84	405	[84]
Al_2O_3	0.5	HDEODA[a] + DPHA[a] + BEA[a]	50	1.38 at 25 s^{-1}	D_p: 124.17	E_c: 13.81	460	[85]
Al_2O_3	1.58	Commercial acrylic resin	80 wt%	≈ 0.12 at 2 s^{-1}	-	-	-	[86]
Al_2O_3	2.3,1.4,0.5	HDDA + PEAAM[a]	10-40	-	-	-	365	[87]
Al_2O_3	9 + 0.05	AM[c] + MBAM[c] + Glycerine + Water	65 wt%	-	-	-	-	[88]
Al_2O_3	0.2	AM + MBAM + Water	30	-	-	-	-	[89]
$\gamma - Al_2O_3$	2-6	Commercial acrylated polysiloxane	34.1 wt%	-	-	-	455-465	[90]
ZrO_2	0.05	ACMO[d] + PEGDA[a]	42	1.68 at 18.6 s^{-1}	D_p: 49.2	E_c: 8.50	405	[61]
ZrO_2	0.2	HDDA + TMPTA	55	1.65 at 200 s^{-1}	-	-	-	[91]
ZrO_2	-	HDDA + IBA[a] + PNPGDA[a]	58	9.02 at 5 s^{-1}	C_d: 99.28	E_{max}: 902.4	375-425	[92]
ZrO_2	0.2	AM + MBAM + Glycerol + Water	40	0.127	-	-	-	[93]
ZrO_2	4.2	Acrylates	50	-	D_p: 50	E_c: 14.94	351-364	[74]
ZrO_2	0.2	HDDA + PPTTA + PEG[e] + U600[a]	60 wt%	-	-	-	-	[1]
SiO_2	5	Acrylic + Silicone acrylate	50	3 at 4 s^{-1}	D_p: 137	E_c: 12.7	325	[94]
SiO_2	2.25	HDDA + PEAAM	40	1.71	D_p: 110	E_c: 18	353	[95]
SiO_2	12	HDDA + EPTA[a]	60	0.58 at 10 s^{-1}	D_p: 805	E_c: 15	355	[96]
SiO_2	3.5	Acrylates	50	-	D_p: 140	E_c: 6.15	351-364	[74]
SiO_2	9.3 + 1.5	AM + MBAM + Glycerol + Water	50	-	$C_d \approx$ 130	E_{max}: 721.89	-	[97]
HA	1	AM + MBAM + Water	52	< 3 at 40 s^{-1}	D_p: 50.7	E_c: 20.3	-	[98]
HA	0.3	Epoxy	60 wt%	< 3 at 100 s^{-1}	D_p: 960	E_c: 25.4	370	[99]
HA	12	Commercial resin	45 wt%	< 3 (at 50 °C)	D_p: 232.4	E_c: 15.06	405	[100]
HA	3	CE[f] + RD[g] + TMPTMA[a]	2.5, 5, 10 wt%	< 3 at 10 s^{-1}	-	-	-	[101]
HA	0.3	Acrylates	55	1.7 at 150 s^{-1}	C_d: 255	E_{max}: 71.5	365	[102]
PZT	5	HDDA + (Epoxy-Acrylate)	45	4.8 at 50 s^{-1}	-	-	351-365	[103]
PZT	3	HDDA + Methacrylate + Acrylate	18	-	C_d: 40	E_{max}: 316	-	[104]
PZT	0.5	HDDA + PEG + U600 + Alcohol	89 wt%	-	-	-	-	[105]
PZT	1-2	Diacrylates	40	0.5	-	E_{max}: 400-800	260-550	[106]
Si_3N_4	0.2	HDDA + TMPTA	-	-	C_d: 51	E_{max}: 500	405	[107]

[a] Acrylate-based monomer.
[b] Polypropylene glycol.
[c] Acrylamide-based monomer.
[d] Acryloyl morpholine.
[e] Pholyethylene glycol.
[f] Epoxy-based monomer.
[g] Reactive diluent.

However, as previously explained, ceramic resins should have high solid loading in the range of 50–65 vol.%, which typically increases the viscosity. This is in contrast to the good homogeneity and low viscosity of the resin [48,56].

Therefore, it is imperative to use a dispersant to manage particle–-particle interactions and maintain a low viscosity if the solid loading of the ceramic powder is more than 35 vol.%. Dispersants are usually used for different purposes, such as stabilizing ceramic suspensions, deagglomerating, and preventing sedimentation [57]. A colloidal dispersant must be carefully selected to disperse the high solid loading of the ceramic powder effectively while maintaining the viscosity below the upper limit [72,54]. The viscosity of 3000 mPa·s at the shear rate of 10 s^{-1} is commonly accepted as an upper limit for a processable ceramic resin used in CSL [48]. Some researchers have claimed that the viscosity of 5000 mPa·s can be considered as the upper limit [56,38]. The upper limit of viscosity is commonly used for the determination of solid loading [48]. Ceramic resins used in CSL should exhibit shear-thinning behavior, which is necessary for the recoating process [72,109]. In general, the rheology of ceramic resins is affected by several parameters, such as, dispersant, solid loading, dilent, particle size and particle shape (BET value). Some of these parameters are in more depth investigated for the preparation of suitable ceramic resins.

4.4.2.1. Dispersant. In a study [56], Hinczewski et al. prepared different slurries containing 53 vol.% alumina in diacrylate monomer solution with different amounts of dispersant. It was observed that the slurries with the dispersant concentration of less than 1.2 wt.% exhibited shear-thickening behavior, which is unfavorable for the CSL process. However, the slurries with dispersant concentration more than 1.2 wt.% exhibited shear-thinning behavior. The minimum viscosity was obtained when 2.2 wt.% dispersant was added to this particular resin. The same procedure has been used in many studies to achieve the minimum viscosity for different ceramic resins and dispersants. This should be noted that, the effect of the dispersant on the resin rheology depends on the ceramic powder properties and the composition of the dispersant and monomer. Therefore, the amount of the dispersant should be carefully selected for each resin.

4.4.2.2. Solid loading. In a study performed by Griffith et al. [72], different solid loadings of silica powder were dispersed in aqueous solutions. It was observed that, as the solid loading was increased, viscosity also increased. The suspension with 50 vol.% solid loading was observed to have the highest solid content whereas it had a viscosity below 3000 mPa.s. The authors also stated that, when silica was dispersed in an acrylate-based resin, solid loadings even below 30 vol.% resulted in viscosities higher than 3000 mPa·s at low shear rates.

In an experimental work by Liao [38], alumina and silica were dispersed in different non-aqueous resins. The same relationship between solid loading and viscosity was observed, which can be justified by the fact that the greater the particle packing in the resin, the more it hinders the resin flow. The prepared 45 vol.% alumina resin and 50 vol.% silica resin had the highest powder content while maintaining viscosities below 5000 mPa·s. The effect of solid loading on resin viscosity has extensively been investigated in other studies as well [98,61]

4.4.2.3. Diluent. Diluents are generally added to resins to reduce the viscosity of the monomer-containing solution, without modifying its reactivity toward UV light. Large addition of diluents (> 40 wt.% of the resin weight) results in the fabrication of soft parts owing to the nature of diluents. In a study by Hinczewski [56], the optimal amount of diluent in the formulation of resin was determined based on the viscosity and UV curability of the highly loaded resins. It was observed that the alumina resin with 80 wt.% solid loading and 30 wt.% diluent (with respect to the resin weight) had the viscosity of 18 Pa·s, which is three times less than the viscosity of the resin without any diluent.

4.4.3. Adequate curing depth

In CSL, ceramic parts are built from layers with a thickness of 10–200 μm. The C_d of the resin must be slightly greater than this range of layer thickness to fabricate a ceramic part within a reasonable time. High spatial resolution is achieved when the resin has a small C_d and C_w. In CSL, it is recommended to have a minimum C_d of 200 μm. However, some researchers have cured layers with a thickness of 150 μm to construct smoother surfaces and finer features at the cost of fast construction [72,33]. As previously discussed, C_d is dependent on the ceramic properties and working parameters, some of which are explained in this section.

4.4.3.1. Refractive index contrast. As indicated by Eq. (7), C_d can be varied by changing Δn as it is inversely proportional to Δn^2. Therefore, the RIs of ceramic powder and resin both affect C_d [59]. Many studies have been conducted with scrupulous attention to the effect of ceramic materials, with varying RI, on the photopolymerization process [110]. It has been proven that the photopolymerization of resins with ceramic materials with low RI, such as SiO_2 (n = 1.56), or medium RI, such as Al_2O_3 (n = 1.70), can be adequately performed. In contrast, the photopolymerization of ceramic materials with high RI, such as Si_3N_4 (n = 2.10) and lead zirconate titanate (PZT) (n = 2.4), is challenging because of their short scattering lengths; consequently, more scattering events occur in the resin medium. This strong scattering effect results in a shallow C_d, which reduces the bonding between the layers, and a broad C_w, which reduces the lateral resolution. The scattering effect can be minimized by using ceramic powders with an RI close to that of the liquid resin [70].

The effect of Δn on the curing profile of a cured line is shown in Fig. 10. This effect was also investigated in a study [111] in which silica suspensions with varying RI for monomer solutions were prepared. It was observed that, at the E_{max} of 203 mJ/cm^2, the ceramic resin with low Δn had larger C_d and smaller C_w, whereas the ceramic resin with high Δn had shallower C_d and larger C_w.

In a study [82], silica (n = 1.46), alumina (n = 1.76), and zirconia (n = 2.05) powders were dispersed in the same liquid resins with solid loading of 60, 60, and 52 vol.%, respectively. It was observed that the zirconia suspension had lower C_d than the silica and alumina suspensions owing to its larger RI. Layer thickness must be chosen appropriately such that it is slightly smaller than C_d to ensure proper bonding between the layers. Therefore, based on the obtained values of C_d in this study, the layer thickness of the silica, alumina, and zirconia suspensions were set to 100, 75, and 25 μm, respectively.

Another study [107] focused on the stereolithographic fabrication of complex ceramic parts with silicon nitride (Si_3N_4) powder, which has a large RI and, therefore, low C_d. The authors claimed that the C_d of the suspension with raw Si_3N_4 powder was 34 μm at the E_{max} of 500 mJ/cm^2. A surface oxidation approach of Si_3N_4 was proposed to improve the C_d. It was observed that, after oxidizing the powder at 1150 and 1200 °C for 1 h, the C_d was effectively increased to 42 and 51 μm, respectively.

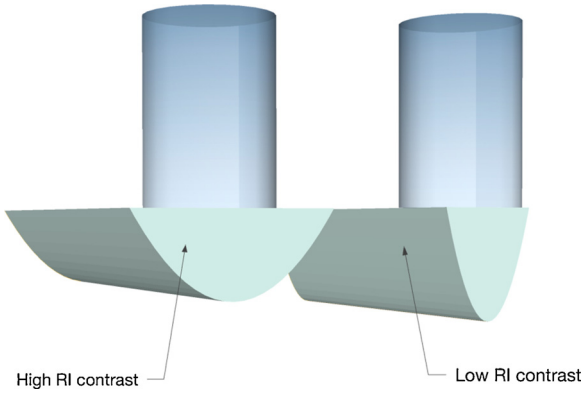

Fig. 10. The schematic view of the curing profile for two ceramic photocurable resins with low and high RI contrast (Δn) being exposed to the same exposure (Inspired by [35]).

However, particular applications require only certain ceramic materials having high RI. In this case, it is possible to reduce the scattering effect by increasing the RI of the resin so that Δn is small [70,112]. A study [72] investigated the effect of different monomer systems with varying RI to achieve a desirable C_d. In this study, 50 vol.% silica powder was loaded in different aqueous solutions with various RIs. It was shown that, as Δn^2 decreased from 0.0317 to 0.0142, C_d increased from 250 to 700 μm at the E_{max} of 1500 mJ/cm^2. In other words, only a small change (4%) in the resin RI resulted in a three-fold increase in C_d.

4.4.3.2. Volume fraction of ceramic powder. As indicated by Eq. (7), C_d is inversely proportional to the volume fraction of ceramic powder. Experimentally, it has also been demonstrated that, by increasing the volume fraction of ceramic powder into the resin, C_d decreases. Griffith et al. [72] prepared photocurable resins by adding different amounts of silica powder into an aqueous solution with the RI of 1.3824. It was observed that, at the E_{max} of 1500 mJ/cm^2, the suspension with 50 vol.% silica powder had a C_d of 360 μm, which is higher than the minimum requirement (200 μm). The C_d decreased to 330 μm when the resin was loaded with 55 vol.% silica powder. The authors also investigated the photopolymerization of a silicon nitride suspension, which had high RI and shallow C_d. The suspension loaded with 10 vol.% ceramic powder had the C_d of 21 μm, whereas it decreased to 10 μm when the suspension was loaded with 20 vol.% ceramic powder. This example proves the challenge of using ceramic materials with high RI in CSL.

4.4.3.3. Particle size and size distribution. According to the light scattering theory, both mean particle size and size distribution of the ceramic powder strongly affect light scattering. Therefore, the resolution of CSL is dependent on the median particle size and distribution of the ceramic powder [31]. Suspensions prepared with coarser particle size have greater C_d compared with suspensions prepared with finer ceramic particles, owing to the lower degree of scattering [113]. Although nanosized powders require lower sintering temperatures and improve the final properties of the end-product, they are unfavorable in terms of C_d [31].

In a study by Sun et al. [], the Monte Carlo simulation was used to model C_d and C_w as a function of mean particle size ranging from 0.3 to 1 μm. It was shown that C_d decreases by reducing the mean particle size. The light scattering effect became significant when the particle

size approached the light wavelength (0.364 μm). Moreover, it was observed that the strong scattering effect caused by broad particle size distribution results in poor spatial resolution. In contrast, the narrow size distribution of ceramic particles is more desired for the fabrication of fine and smooth surfaces [70].

In contrast, in an experimental study by Griffith et al. [72], different grades (0.46 and 0.61 μm) of alumina powder were used to determine the effect of particle size on C_d. It was shown that both suspensions with 50 vol% solid loading had C_d greater than 200 μm. However, the suspension with the smaller particle size had a larger C_d, i.e., 400 versus 300 μm. This result could not be reconciled with simple scattering theories, such as the Rayleigh–Gans theory and Mie theory, which relate particle size to light scattering for very dilute suspensions. The authors empirically discovered that, for highly concentrated suspensions, C_d is strongly affected by β in Eq. (7), which is related to the square of particle size (d^2). Therefore, the authors stated that C_d is inversely proportional to particle size for highly concentrated resins.

4.4.3.4. Photoinitiator. C_d is often considered to be synonymous with monomer-to-polymer conversion. Literature shows that, as the PI concentration increases, conversion and C_d increase. In the case of low PI concentrations, the conversion to polymer is too low to form a gel; therefore, C_d approaches zero. At the other extreme of high PI concentrations, the penetration depth of photons decreases. Therefore, there must be an intermediate optimal concentration to achieve adequate C_d [114]. Chartier et al. [74] evaluated the influence of the PI concentration on the C_d of alumina, silica, and zirconia suspensions with different PI concentrations ranging from 0.3 to 1 wt.% (with respect to the monomer weight). The result of this study showed no significant effect of the PI concentration on the C_d and C_w of the prepared suspensions. However, the laser beam was highly absorbed by the quickly polymerized surface at high PI concentrations (> 2 wt.%).

4.4.3.5. Energy dose. The effect of E_{max} on the curing profile was investigated in a study by Gentry et al. [68]. It was shown that, by increasing the E_{max} (54, 203, and 608 mJ/cm^2), both the C_d and C_d of the silica suspension with low Δn were increased. In another study [115], three different acrylate monomers were loaded with 60 vol.% silica powder. It was concluded that one way to increase C_d is to increase E_{max}. Another study [29] investigated the same effect and showed that both C_d and C_w were decreased as E_{max} was decreased by increasing the scanning speed. When the E_{max} was decreased from 15387.7 to 76.9 mJ/cm^2, C_d decreased from 244.00 to 85.60 μm, and C_w also decreased from 1051.31 to 153.58 μm. Another work [74] showed that the dimensional resolution of the printed parts can be increased by decreasing the E_{max} of the applied laser.

5. Ceramic stereolithography market: its current status, challenges, and future

The market for additively manufactured high-performance ceramic parts is relatively new and rapidly growing. Companies developing ceramic resins and providing manufacturing services have realized the ability of the CSL technique to produce ceramic parts with complex geometries, which can be used in different industries, such as aerospace, jewelry, electronics, dental, and biomedical fields. Therefore, significant investments are being made by the major suppliers of SLA systems in the market of CSL, such as 3DCeram Sinto, Lithoz, Admatec, and Prodways. Table 2 summarizes the main features of some of the SLA systems manufactured by these companies. Moreover, these companies offer ready-to-use ceramic resins for sale, some of which are mentioned in this table.

Although CSL is considered to provide the highest resolution among ceramic AM techniques, it suffers from considerable limitations. Despite the increasing number of available ceramic resins in the market, this technique is still restricted to the use of one resin at a time, which ultimately limits its potential applications. In fact, there are activities to use multiple resins at a time, however, it requires complex sequential polymerization and cleaning steps between the material changes [19].

Moreover, the manufacturing time of the conventional SLA printers is relatively long. Several approaches have been proposed to solve this issue. The scanning process itself in SSL systems restricts the decrease in the manufacturing time. This could be overcome by using precise and narrow scanning patterns only for areas where high resolution is required while using a broader scanning pattern for bulk features. The combination of SSL and PSL techniques is currently being developed and explored. These hybrid systems can further reduce the manufacturing time to rates similar to PSL while maintaining the high precision of laser illumination [116].

The printing resolution of PSL is dependent on the size of the micromirrors in DMD and the optical system. Generally, a higher resolution can be more easily achieved in a smaller printing area by using suitable optics. Therefore, the size of the building platforms used in such systems is relatively small. Hybrid systems can lead to a compromise between the size of the building platform and resolution. The large–area projection micro-stereolithography (LAPμ SL) is an image projection micro-stereolithography system that produces very small features over large areas rapidly. LAPμSL combines the advantages of SSL (large area but poor resolution) and PSL (high resolution but only over a small area), enabling the rapid printing of fine details over large areas. This technology uses optical techniques to write images in parallel by moving the DMD, in contrast to other competing technologies, which either require the rastering of beams to expose pixels in series or mechanical stage moves. Thus, centimeter-sized components with a micrometer-range resolution can be fabricated at a low cost. It is believed that these hybrid systems can expand the application range of CSL in the future after thorough investigation and development [14,116].

6. Conclusion

Among AM techniques, CSL is most widely used for the fabrication of ceramic parts owing to its high accuracy in printing complex geometries. SLA fabricates a 3D ceramic structure by printing layers of ceramic resin successively. Each 2D layer of the liquid ceramic resin, with a defined thickness between 25 and 100 μm, is exposed to the laser irradiation source and then becomes solidified. The solidification process is based on the photopolymerization of the liquid resin, which consists of a ceramic powder, an organic monomer, such as acrylate and epoxy, PIs, and other additives to achieve desirable properties. Once each layer of resin is exposed to UV light, the laser beam supplies the energy required to induce photopolymerization and photocrosslinking. The fabricated 3D structure is referred to as a composite green body consisting of polymer and ceramic. The green body undergoes debinding to burn out the contained polymer and achieve a pure ceramic part. This process is followed by sintering to obtain a dense ceramic part.

A critical step in CSL is to prepare a suitable ceramic resin for printing. The fine ceramic powder should be homogenously mixed with a monomer-containing solution, which often requires the addition of a dispersant to maintain the resin stability. A suitable photocurable ceramic resin used in CSL should satisfy a few requirements. First, the solid loading of the ceramic powder should be more than 40 vol% to avoid excessive shrinkage and delamination during the debinding and sintering processes. Second, the ceramic resin must be highly mobile for the fabrication of ceramic parts via SLA within an optimum manufacturing time. Typically, it is recommended that the ceramic resin should have low viscosity below 3000 *mPa. s* to ensure the self-leveling and recoating of the resin. Third, it is highly recommended that the C_d of a highly loaded suspension should be equal to or greater than 150–200 μm after being exposed to UV radiation. C_d is one of the most important parameters in CSL because it strongly affects the vertical and

Table 2
The main features of the SLA systems made by 3DCeram Sinto, Lithoz, Admatec and Prodways.

Properties	3DCeram Sinto	Lithoz	Admatec	Prodways
	(C900 Flex)	(CeraFab)	(Admaflex 130)	(Promaker V6000)
Printing technology	DLP [a] (top-down)	LCM [b] (bottom-up)	DLP (bottom-up)	DLP (top-down)
Machine size ($D \times W \times H$ m^3)	$2.2 \times 1.06 \times 2.04$	$1.2 \times 0.6 \times 1.8$	$0.5 \times 0.8 \times 1.7$	$1.8 \times 1.1 \times 1.8$
Building platform size ($D \times W \times H$ mm^3)	$100 \times 300 \times 100$ $200 \times 300 \times 100$ $300 \times 300 \times 100$	$76 \times 43 \times 170$ $115 \times 64 \times 200$	$90 \times 56 \times 110$ $160 \times 100 \times 110$	$120 \times 150 \times 150$ $120 \times 350 \times 150$ $120 \times 550 \times 150$
Layer thickness (μm)	10-125	10-100	10-200	25-150
Lateral resolution (μm)	35	40/60	35/62.5	32
Light source	UV laser	LED	UV laser	LED
Weight (kg)	1450	250	300	800
Power requirement (V)	220-240	220	230	210-240
Ready-to-use resins	Al_2O_3 ZrO_2 HA - SiO_2 Si_3N_4	Al_2O_3 ZrO_2 HA $Ca_3(PO_4)_2$ [c] SiO_2-based Si_3N_4	Al_2O_3 ZrO_2 - - SiO_2 -	Al_2O_3 ZrO_2 HA $Ca_3(PO_4)_2$ - -

[a] Digital light processing.
[b] Lithography-based ceramic manufacturing.
[c] Calcium phosphate.

lateral resolutions. This parameter is defined as the depth at which the gel point is achieved and is strongly affected by the scattering phenomenon owing to the presence of ceramic particles. The scattering phenomenon is dependent on the median particle size, volume fraction, and RI of the powder. Therefore, the same variables control C_d.

Acknowledgments

We would like to express our sincere gratitude to Finnish Cultural Foundation, the graduate school ofTampere University, European Regional Development Fund and Council of Tampere Regionfor supporting and funding our research in the field of ceramic stereolithography.

References

[1] R. He, W. Liu, Z. Wu, D. An, M. Huang, H. Wu, Q. Jiang, X. Ji, S. Wu, Z. Xie, Fabrication of complex-shaped zirconia ceramic parts via a DLP-stereolithography-based 3D printing method, Ceram. Int. 44 (3) (2018) 3412–3416, https://doi.org/10.1016/j.ceramint.2017.11.135.
[2] R. Janssen, S. Scheppokat, N. Claussen, Tailor-made ceramic-based components-advantages by reactive processing and advanced shaping techniques, J. Eur. Ceram. Soc. 28 (7) (2008) 1369–1379, https://doi.org/10.1016/j.jeurceramsoc.2007.12.022.
[3] H. Wu, W. Liu, R. He, Z. Wu, Q. Jiang, X. Song, Y. Chen, L. Cheng, S. Wu, Fabrication of dense zirconia-toughened alumina ceramics through a stereolithography-based additive manufacturing, Ceram. Int. 43 (1) (2017) 968–972, https://doi.org/10.1016/j.ceramint.2016.10.027.
[4] K. Zhang, C. Xie, G. Wang, R. He, G. Ding, M. Wang, D. Dai, D. Fang, High solid loading, low viscosity photosensitive Al2O3 slurry for stereolithography based additive manufacturing, Ceram. Int. 45 (1) (2019) 203–208, https://doi.org/10.1016/j.ceramint.2018.09.152.
[5] W. Chen, F. Wang, K. Yan, Y. Zhang, D. Wu, Micro-stereolithography of KNN-based lead-free piezoceramics, Ceram. Int. 45 (4) (2019) 4880–4885, https://doi.org/10.1016/j.ceramint.2018.11.185.
[6] Z. Xing, W. Liu, Y. Chen, W. Li, Effect of plasticizer on the fabrication and properties of alumina ceramic by stereolithography-based additive manufacturing, Ceram. Int. 44 (16) (2018) 19939–19944, https://doi.org/10.1016/j.ceramint.2018.07.259.
[7] I. Gibson, D.W. Rosen, B. Stucker, Additive Manufacturing Technologies, Springer, New York, 2014, https://doi.org/10.1007/978-1-4939-2113-3.
[8] T.D. Ngo, A. Kashani, G. Imbalzano, K.T. Nguyen, D. Hui, Additive manufacturing (3D printing): A review of materials, methods, applications and challenges, Compos. Part B-Eng. 143 (2018) 172–196, https://doi.org/10.1016/j.compositesb.2018.02.012.
[9] J.C. Ruiz-Morales, A. Tarancón, J. Canales-Vázquez, J. Méndez-Ramos, L. Hernández-Afonso, P. Acosta-Mora, J.M. Rueda, R. Fernández-González, Three dimensional printing of components and functional devices for energy and environmental applications, Energy Environ. Sci. 10 (4) (2017) 846–859, https://doi.org/10.1039/C6EE03526D.
[10] E.M. Hernández-Rodríguez, P. Acosta-Mora, J. Méndez-Ramos, E.B. Chinea, P.E. Ferrera, J. Canales-Vázquez, P. Núñez, J.C. Ruiz-Morales, Prospective use of the 3D printing technology for the microstructural engineering of solid oxide fuel cell components, Bol. Soc. Esp. Ceram. Vidr. 3 (5) (2014) 213–216, https://doi.org/10.3989/cyv.252014.
[11] T. Hafkamp, G. van Baars, B. de Jager, P. Etman, A feasibility study on process monitoring and control in vat photopolymerization of ceramics, Mechatronics 56 (2018) 220–241, https://doi.org/10.1016/j.mechatronics.2018.02.006.
[12] L. L”u, J.Y. Fuh, Y.S. Wong, Fundamentals of Laser-Lithography Processes, Laser-Induced Materials and Processes for Rapid Prototyping, Springer, Boston, 2001, pp. 9–38, https://doi.org/10.1007/978-1-4615-1469-5_2.
[13] P.J. Bártolo (Ed.), Stereolithography: Materials, Processes and Applications, Springer Science & Business Media, 2011, , https://doi.org/10.1007/978-0-387-92904-0.
[14] J.Z. Manapat, Q. Chen, P. Ye, R.C. Advincula, 3D printing of polymer nanocomposites via stereolithography, Macromol. Mater. Eng. 302 (9) (2017 Sep) 1600553, https://doi.org/10.1002/mame.201600553.
[15] G. Mitteramskogler, R. Gmeiner, R. Felzmann, S. Gruber, C. Hofstetter, J. Stampfl, J. Ebert, W. Wachter, J. Laubersheimer, Light curing strategies for lithography-based additive manufacturing of customized ceramics, Addit. Manuf. 1 (2014) 110–118, https://doi.org/10.1016/j.addma.2014.08.003.
[16] J.W. Lee, I.H. Lee, D.W. Cho, Development of micro-stereolithography technology using metal powder, Microelectron. Eng. 83 (4–9) (2006) 1253–1256, https://doi.org/10.1016/j.mee.2006.01.192.
[17] F. Liravi, S. Das, C. Zhou, Separation force analysis and prediction based on cohesive element model for constrained-surface Stereolithography processes, Comput. Aided. Design 69 (2015) 134–142, https://doi.org/10.1016/j.cad.2015.05.002.
[18] D.W. Hutmacher, M. Sittinger, M.V. Risbud, Scaffold-based tissue engineering: rationale for computer-aided design and solid free-form fabrication systems, Trends. Biotechnol. 22 (7) (2004) 354–362, https://doi.org/10.1016/j.tibtech.2004.05.005.
[19] F.P. Melchels, J. Feijen, D.W. Grijpma, A review on stereolithography and its applications in biomedical engineering, Biomaterials 31 (24) (2010) 6121–6130, https://doi.org/10.1016/j.biomaterials.2010.04.050.
[20] C. Sun, N. Fang, D.M. Wu, X. Zhang, Projection micro-stereolithography using digital micro-mirror dynamic mask, Sensor. Actuat. A-Phys. 121 (1) (2005) 113–120, https://doi.org/10.1016/j.sna.2004.12.011.
[21] P.F. Jacobs, Rapid Prototyping & Manufacturing: Fundamentals of Stereolithography, Society of Manufacturing Engineers, 1992.
[22] H. Yao, J. Wang, S. Mi, Photo processing for biomedical hydrogels design and functionality: A review, Polymers 10 (1) (2017 Dec 22) 11, https://doi.org/10.3390/polym10010011.
[23] J.R. Tumbleston, D. Shirvanyants, N. Ermoshkin, R. Janusziewicz, A.R. Johnson, D. Kelly, K. Chen, R. Pinschmidt, J.P. Rolland, A. Ermoshkin, E.T. Samulski, Continuous liquid interface production of 3D objects, Science 347 (6228) (2015) 1349–1352, https://doi.org/10.1126/science.aaa2397.
[24] X. Song, Y. Chen, T.W. Lee, S. Wu, L. Cheng, Ceramic fabrication using mask-image-projection-based stereolithography integrated with tape-casting, J. Manuf. Process. 20 (2015) 456–464, https://doi.org/10.1016/j.jmapro.2015.06.022.
[25] Y. Pan, C. Zhou, Y. Chen, Rapid manufacturing in minutes: the development of a

mask projection stereolithography process for high-speed fabrication, ASME 2012 International Manufacturing Science and Engineering Conference collocated with the 40th North American Manufacturing Research Conference and in participation with the International Conference on Tribology Materials and Processing (2012 Jun 4) 405–414, https://doi.org/10.1115/MSEC2012-7232.
[26] H. Rayat, V. Pulkkinen, M. Johansson, V. Nyfors, J. Partanen, P. Kuosmanen, The Effects of Minituarisation Of Projection Stereolithography Equipment on Printing Quality. Proc. of 9th International DAAM Baltic Conference (2014) 278–282.
[27] C. Zhou, Y. Chen, Z. Yang, B. Khoshnevis, Digital material fabrication using mask-image-projection-based stereolithography, Rapid. Prototyp. J. 19 (3) (2013) 153–165, https://doi.org/10.1108/13552541311312148.
[28] Y.M. Huang, C.P. Jiang, On-line force monitoring of platform ascending rapid prototyping system, Journal of materials processing technology, J. Mater. Process. Tech. 159 (2) (2005) 257–264, https://doi.org/10.1016/j.jmatprotec.2004.05.015.
[29] Z. Chen, D. Li, W. Zhou, L. Wang, Curing characteristics of ceramic stereolithography for an aqueous-based silica suspension, Proc. Inst. Mech. Eng. B J. Eng. Manuf. 224 (4) (2010) 641–651, https://doi.org/10.1243/09544054JEM1751.
[30] S.H. Lee, W.S. Park, H.S. Cho, W. Zhang, M.C. Leu, A neural network approach to the modelling and analysis of stereolithography processes, Proc. Inst. Mech. Eng. B J. Eng. Manuf. 215 (12) (2001) 1719–1733, https://doi.org/10.1177/095440540121501206.
[31] J. Tarabeux, V. Pateloup, P. Michaud, T. Chartier, Development of a numerical simulation model for predicting the curing of ceramic systems in the stereolithography process, J. Eur. Ceram. Soc. 38 (11) (2018) 4089–4098, https://doi.org/10.1016/j.jeurceramsoc.2018.03.052.
[32] P.F. Jacobs, Fundamentals of stereolithography, 1992 International Solid Freeform Fabrication Symposium (1992).
[33] X. Zhang, X.N. Jiang, C. Sun, Micro-stereolithography of polymeric and ceramic microstructures, Sensor. Actuat. A-Phys. 77 (2) (1999) 149–156, https://doi.org/10.1016/S0924-4247(99)00189-2.
[34] J.W. Choi, R.B. Wicker, S.H. Cho, C.S. Ha, S.H. Lee, Cure depth control for complex 3D microstructure fabrication in dynamic mask projection micro-stereolithography, Rapid. Prototyp. J. 15 (1) (2009) 59–70, https://doi.org/10.1108/13552540910925072.
[35] J.W. Halloran, Ceramic stereolithography: additive manufacturing for ceramics by photopolymerization, Annu. Rev. Mater. Res. 46 (2016) 19–40, https://doi.org/10.1146/annurev-matsci-070115-031841.
[36] M. Wu, W. Zhao, Y. Tang, D. Li, B. Lu, A novel stereolithography technology with conventional UV light, Rapid. Prototyp. J. 7 (5) (2001) 268–275, https://doi.org/10.1108/EUM0000000006117.
[37] R.B. Gowda, C.S. Udayagiri, D.D. Narendra, Studies on the process parameters of rapid prototyping technique (Stereolithography) for the betterment of part quality, IJME (2014) 2014, https://doi.org/10.1155/2014/804705.
[38] H. Liao, Stereolithography using Compositions Containing Ceramic Powders, University of Toronto;, 1998.
[39] S.O. Onuh, K.K. Hon, Optimising build parameters and hatch style for part accuracy in stereolithography, 1997 International Solid Freeform Fabrication Symposium (1997) 11–13.
[40] M. Tehfe, F. Louradour, J. Lalevée, J.P. Fouassier, Photopolymerization reactions: On the way to a green and sustainable chemistry, Appl. Sci. 3 (2) (2013) 490–514, https://doi.org/10.3390/app3020490.
[41] J.P. Fouassier, J. Lalevée, Photoinitiators for Polymer Synthesis: Scope, Reactivity, and Efficiency, John Wiley & Sons, 2012.
[42] I.V. Khudyakov, Fast photopolymerization of acrylate coatings: Achievements and problems, Prog. Org. Coat. 121 (2018) 151–159, https://doi.org/10.1016/j.porgcoat.2018.04.030.
[43] R. NOMOTO, Effect of light wavelength on polymerization of light-cured resins, Dent. Mater. J. 16 (1) (1997) 60–73, https://doi.org/10.4012/dmj.16.60.
[44] A. Atala, J.J. Yoo, Essentials of 3D Biofabrication and Translation, Academic Press, 2015.
[45] E. Andrzejewska, M. Andrzejewski, Polymerization kinetics of photocurable acrylic resins, J. Polym. Sci. Pol. Chem. 36 (4) (1998) 665–673 https://doi.org/10.1002/(SICI)1099-0518(199803)36:4 < 665::AID-POLA15 > 3.0.CO;2-K.
[46] J.P. Fouassier, Photoinitiation, Photopolymerization, and Photocuring: Fundamentals and Applications, Hanser, 1995.
[47] T.N. Eren, N. Okte, F. Morlet Savary, J.P. Fouassier, J. Lalevee, D. Avci, One component thioxanthone based polymeric photoinitiators, J. Polym. Sci. Pol. Chem. 54 (20) (2016) 3370–3378, https://doi.org/10.1002/pola.28227.
[48] C.J. Bae, A. Ramachandran, K. Chung, S. Park, Ceramic stereolithography: additive manufacturing for 3D complex ceramic structures, J. Korean. Ceram. Soc. 54 (6) (2017) 470–477, https://doi.org/10.4191/kcers.2017.54.6.12.
[49] N.S. Allen, Photoinitiators for UV and visible curing of coatings: mechanisms and properties, J. Photochem. Photobiol. A Chem. 100 (1–3) (1996) 101–107, https://doi.org/10.1016/S1010-6030(96)04426-7.
[50] V. Sipani, A.B. Scranton, Photopolymerization Cationic, Encycl Polym. Sci. Technol. (2002), https://doi.org/10.1002/0471440264.pst491.
[51] Fan RN, inventor; EI du Pont de Nemours and Co, assignee. Solid imaging method using photohardenable compositions containing hollow spheres, United States patent US 5,051,334, 1991 Sep 24.
[52] L. Ferrage, G. Bertrand, P. Lenormand, D. Grossin, B. Ben-Nissan, A review of the additive manufacturing (3DP) of bioceramics: alumina, zirconia (PSZ) and hydroxyapatite, J. Aust. Ceram. Soc. 53 (1) (2017) 11–20, https://doi.org/10.1007/s41779-016-0003-9.
[53] S. Mansour, M. Gilbert, R. Hague, A study of the impact of short-term ageing on the mechanical properties of a stereolithography resin, Mater. Sci. Eng. A. 447 (1–2) (2007) 277–284, https://doi.org/10.1016/j.msea.2006.10.007.
[54] W. Zimbeck, R. Rice, Stereolithography of Ceramics and Metals, IS and T Annual Conference, The Society for Imaging Science and Technology, 1997, pp. 649–655.
[55] F.P. Melchels, Preparation of Advanced Porous Structures by Stereolithography for Application in Tissue Engineering, University of Twente, Enschede, The Netherlands, 2010 Feb.
[56] C. Hinczewski, S. Corbel, T. Chartier, Ceramic suspensions suitable for stereolithography, J. Eur. Ceram. Soc 18 (6) (1998) 583–590, https://doi.org/10.1016/S0955-2219(97)00186-6.
[57] C. Chaput, T. Chartier, Fabrication of ceramics by stereolithography, RTejournal-Forum für Rapid Technologie 4 (1) (2007 Aug 29).
[58] Halloran JW, Griffith M, Chu TM, inventors; University of Michigan, assignee. Stereolithography resin for rapid prototyping of ceramics and metals. United States patent US 6,117,612. 2000 Sep 12.
[59] M.L. Griffith, J.W. Halloran, Ultraviolet curing of highly loaded ceramic suspensions for stereolithography of ceramics, 1994 International Solid Freeform Fabrication Symposium (1994 Sep) 396–403.
[60] F. Azarmi, A. Amiri, Microstructural evolution during fabrication of alumina via laser stereolithography technique, Ceram. Int. 45 (1) (2019) 271–278, https://doi.org/10.1016/j.ceramint.2018.09.163.
[61] J. Sun, J. Binner, J. Bai, Effect of surface treatment on the dispersion of nano zirconia particles in non-aqueous suspensions for stereolithography, J. Eur. Ceram. Soc. 39 (4) (2019) 1660–1667, https://doi.org/10.1016/j.jeurceramsoc.2018.10.024.
[62] D. Komissarenko, P. Sokolov, A. Evstigneeva, I. Shmeleva, A. Dosovitsky, Rheological and curing behavior of acrylate-based suspensions for the DLP 3D printing of complex zirconia parts, Materials 11 (12) (2018) 2350, https://doi.org/10.3390/ma11122350.
[63] C. Liu, B. Qian, X. Liu, L. Tong, J. Qiu, Additive manufacturing of silica glass using laser stereolithography with a top-down approach and fast debinding, RSC. Adv. 8 (29) (2018) 16344–16348, https://doi.org/10.1039/C8RA02428F.
[64] Y.Y. Wang, L. Li, Z.Y. Wang, F.T. Liu, J.H. Zhao, P.P. Zhang, C. Lu, Fabrication of Dense Silica Ceramics through a Stereo Lithography-Based Additive Manufacturing, Solid. State. Phenom. 281 (2018) 456–462 https://doi.org/10.4028/www.scientific.net/SSP.281.456.
[65] F. Kotz, D. Helmer, B.E. Rapp, Additive manufacturing of microfluidic glass chips, Proc. SPIE 10491, Microfluidics, BioMEMS, and Medical Microsystems XVI 10491 (2018) 104910A, https://doi.org/10.1117/12.2287654.
[66] Y. de Hazan, D. Penner, SiC and SiOC ceramic articles produced by stereolithography of acrylate modified polycarbosilane systems, J. Eur. Ceram. Soc. 37 (16) (2017) 5205–5212, https://doi.org/10.1016/j.jeurceramsoc.2017.03.021.
[67] V. Tomeckova, J.W. Halloran, Cure depth for photopolymerization of ceramic suspensions, J. Eur. Ceram. Soc. 30 (15) (2010) 3023–3033, https://doi.org/10.1016/j.jeurceramsoc.2010.06.004.
[68] S.P. Gentry, J.W. Halloran, Depth and width of cured lines in photopolymerizable ceramic suspensions, J. Eur. Ceram. Soc. 33 (10) (2013) 1981–1988, https://doi.org/10.1016/j.jeurceramsoc.2013.02.033.
[69] B. Pick, C.C. Gonzaga, W.S. Junior, Y. Kawano, R.R. Braga, P.E. Cardoso, Influence of curing light attenuation caused by aesthetic indirect restorative materials on resin cement polymerization, Eur. J. Dent. 4 (3) (2010) 314 PubMed PMID: 20613921; PubMed Central PMCID: PMC2897866.
[70] C. Sun, X. Zhang, Experimental and numerical investigations on micro-stereolithography of ceramics, J. Appl. Phys. 92 (8) (2002) 4796–4802, https://doi.org/10.1063/1.1503410.
[71] J.W. Halloran, V. Tomeckova, S. Gentry, S. Das, P. Cilino, D. Yuan, R. Guo, A. Rudraraju, P. Shao, T. Wu, T.R. Alabi, Photopolymerization of powder suspensions for shaping ceramics, J. Eur. Ceram. Soc. 31 (14) (2011) 2613–2619, https://doi.org/10.1016/j.jeurceramsoc.2010.12.003.
[72] M.L. Griffith, J.W. Halloran, Freeform fabrication of ceramics via stereolithography, J. Am. Ceram. Soc. 79 (10) (2020) 2601–2608, https://doi.org/10.1111/j.1151-2916.1996.tb09022.x.
[73] G.A. Brady, T.M. Chu, J.W. Halloran, Curing behavior of ceramic resin for stereolithography, 1996 International Solid Freeform Fabrication Symposium (1996) 403–405.
[74] T. Chartier, C. Chaput, F. Doreau, M. Loiseau, Stereolithography of structural complex ceramic parts, J. Mater. Sci. 37 (15) (2002) 3141–3147, https://doi.org/10.1023/A:101610221.
[75] B. Sager, D.W. Rosen, M. Shilling, T.R. Kurfess, Experimental studies in stereolithography resolution, Proceedings of the Solid Freeform Fabrication Symposium (2003) 70–81.
[76] W. Miao, J.W. Halloran, D.E. Brei, Suspension polymerization casting of lead zirconate titanate, part I: Acrylamide hydrogel system, J. Mater. Sci. 38 (12) (2003) 2571–2579, https://doi.org/10.1023/A:102446601.
[77] W. Zhou, D. Li, H. Wang, A novel aqueous ceramic suspension for ceramic stereolithography, Rapid. Prototyp. J. 16 (1) (2010) 29–35, https://doi.org/10.1108/13552541011011686.
[78] X. Wu, Q. Lian, D. Li, X. He, J. Meng, X. Liu, Z. Jin, Influence of boundary masks on dimensions and surface roughness using segmented exposure in ceramic 3D printing, Ceram. Int. 45 (3) (2019) 3687–3697, https://doi.org/10.1016/j.ceramint.2018.11.031.
[79] S. Zhang, N. Sha, Z. Zhao, Surface modification of α-Al2O3 with dicarboxylic acids for the preparation of UV-curable ceramic suspensions, J. Eur. Ceram. Soc. 37 (4) (2017) 1607–1616, https://doi.org/10.1016/j.jeurceramsoc.2016.12.013.
[80] X. Li, K. Hu, Z. Lu, Effect of light attenuation on polymerization of ceramic suspensions for stereolithography, J. Eur. Ceram. Soc. 39 (7) (2019) 2503–2509,

https://doi.org/10.1016/j.jeurceramsoc.2019.01.002.
[81] A. Goswami, K. Ankit, N. Balashanmugam, A.M. Umarji, G. Madras, Optimization of rheological properties of photopolymerizable alumina suspensions for ceramic microstereolithography, Ceram. Int. 40 (2) (2014) 3655–3665, https://doi.org/10.1016/j.ceramint.2013.09.059.
[82] K. Hu, Y. Wei, Z. Lu, L. Wan, P. Li, Design of a shaping system for stereolithography with high solid loading ceramic suspensions, 3D Print. Addit. Manuf. 5 (4) (2018) 311–318, https://doi.org/10.1089/3dp.2017.0065.
[83] T. Chartier, C. Dupas, P.M. Geffroy, V. Pateloup, M. Colas, J. Cornette, S. Guillemet-Fritsch, Influence of irradiation parameters on the polymerization of ceramic reactive suspensions for stereolithography, J. Eur. Ceram. Soc. 37 (15) (2017) 4431–4436, https://doi.org/10.1016/j.jeurceramsoc.2017.05.050.
[84] K. Li, Z. Zhao, The effect of the surfactants on the formulation of UV-curable SLA alumina suspension, Ceram. Int. 43 (6) (2017) 4761–4767, https://doi.org/10.1016/j.ceramint.2016.11.143.
[85] E. Johansson, O. Lidström, J. Johansson, O. Lyckfeldt, E. Adolfsson, Influence of resin composition on the defect formation in alumina manufactured by stereolithography, Materials 10 (2) (2017) 138, https://doi.org/10.3390/ma10020138.
[86] M. Dehurtevent, L. Robberecht, J.C. Hornez, A. Thuault, E. Deveaux, P. Béhin, Stereolithography: a new method for processing dental ceramics by additive computer-aided manufacturing, Dent. Mater. 33 (5) (2017) 477–485, https://doi.org/10.1016/j.dental.2017.01.018.
[87] A. Badev, Y. Abouliatim, T. Chartier, L. Lecamp, P. Lebaudy, C. Chaput, C. Delage, Photopolymerization kinetics of a polyether acrylate in the presence of ceramic fillers used in stereolithography, J. Photochem. Photobiol. A Chem. 222 (1) (2011) 117–122, https://doi.org/10.1016/j.jphotochem.2011.05.010.
[88] H. Wu, Y. Cheng, W. Liu, R. He, M. Zhou, S. Wu, X. Song, Y. Chen, Effect of the particle size and the debinding process on the density of alumina ceramics fabricated by 3D printing based on stereolithography, Ceram. Int. 42 (15) (2016) 17290–17294, https://doi.org/10.1016/j.ceramint.2016.08.024.
[89] M. Zhou, W. Liu, H. Wu, X. Song, Y. Chen, L. Cheng, F. He, S. Chen, S. Wu, Preparation of a defect-free alumina cutting tool via additive manufacturing based on stereolithography-Optimization of the drying and debinding processes, Ceram. Int. 42 (10) (2016) 11598–11602, https://doi.org/10.1016/j.ceramint.2016.04.050.
[90] J. Schmidt, A.A. Altun, M. Schwentenwein, P. Colombo, Complex mullite structures fabricated via digital light processing of a preceramic polysiloxane with active alumina fillers, J. Eur. Ceram. Soc. 39 (4) (2019) 1336–1343, https://doi.org/10.1016/j.jeurceramsoc.2018.11.038.
[91] K. Zhang, R. He, C. Xie, G. Wang, G. Ding, M. Wang, W. Song, D. Fang, Photosensitive ZrO2 suspensions for stereolithography, Ceram. Int. 45 (9) (2019) 12189–12195, https://doi.org/10.1016/j.ceramint.2019.03.123.
[92] K.J. Jang, J.H. Kang, J.G. Fisher, S.W. Park, Effect of the volume fraction of zirconia suspensions on the microstructure and physical properties of products produced by additive manufacturing, Dent. Mater. 35 (5) (2019) e97–e106, https://doi.org/10.1016/j.dental.2019.02.001.
[93] Q. Lian, W. Sui, X. Wu, F. Yang, S. Yang, Additive manufacturing of ZrO2 ceramic dental bridges by stereolithography, Rapid. Prototyp. J. 24 (1) (2018) 114–119, https://doi.org/10.1108/RPJ-09-2016-0144.
[94] C.E. Corcione, A. Greco, F. Montagna, A. Licciulli, A. Maffezzoli, Silica moulds built by stereolithography, J. Mater. Sci. 40 (18) (2005) 4899–4904, https://doi.org/10.1007/s10853-005-3888-1.
[95] T. Chartier, A. Badev, Y. Abouliatim, P. Lebaudy, L. Lecamp, Stereolithography process: influence of the rheology of silica suspensions and of the medium on polymerization kinetics-cured depth and width, J. Eur. Ceram. Soc. 32 (8) (2012) 1625–1634, https://doi.org/10.1016/j.jeurceramsoc.2012.01.010.
[96] C.J. Bae, J.W. Halloran, Integrally cored ceramic mold fabricated by ceramic stereolithography, Int. J. Appl. Ceram. Technol. 8 (6) (2011) :1255–:1262, https://doi.org/10.1111/j.1744-7402.2010.02568.x.
[97] W. Zhou, D. Li, Z. Chen, The influence of ingredients of silica suspensions and laser exposure on UV curing behavior of aqueous ceramic suspensions in stereolithography, Int. J. Adv. Manuf. Technol. 52 (5–8) (2011) 575–582, https://doi.org/10.1007/s00170-010-2746-8.
[98] Z. Wang, C. Huang, J. Wang, B. Zou, Development of a novel aqueous hydroxyapatite suspension for stereolithography applied to bone tissue engineering, Ceram. Int. 45 (3) (2019) 3902–3909, https://doi.org/10.1016/j.ceramint.2018.11.063.
[99] F. Scalera, C.E. Corcione, F. Montagna, A. Sannino, A. Maffezzoli, Development and characterization of UV curable epoxy/hydroxyapatite suspensions for stereolithography applied to bone tissue engineering, Ceram. Int. 40 (10) (2014) 15455–15462, https://doi.org/10.1016/j.ceramint.2014.06.117.
[100] Z. Liu, H. Liang, T. Shi, D. Xie, R. Chen, X. Han, L. Shen, C. Wang, Z. Tian, Additive manufacturing of hydroxyapatite bone scaffolds via digital light processing and in vitro compatibility, Ceram. Int. 45 (8) (2019) 11079–11086, https://doi.org/10.1016/j.ceramint.2019.02.195.
[101] P. Makvandi, C. Esposito Corcione, F. Paladini, A.L. Gallo, F. Montagna, R. Jamaledin, M. Pollini, A. Maffezzoli, Antimicrobial modified hydroxyapatite composite dental bite by stereolithography, Polym. Adv. Technol. 29 (1) (2018) 364–371, https://doi.org/10.1002/pat.4123.
[102] M. Lasgorceix, E. Champion, T. Chartier, Shaping by microstereolithography and sintering of macro-micro-porous silicon substituted hydroxyapatite, J. Eur. Ceram. Soc. 36 (4) (2016) 1091–1101, https://doi.org/10.1016/j.jeurceramsoc.2015.11.020.
[103] O. Dufaud, P. Marchal, S. Corbel, Rheological properties of PZT suspensions for stereolithography, J. Eur. Ceram. Soc. 22 (13) (2002) 2081–2092, https://doi.org/10.1016/S0955-2219(02)00036-5.
[104] Y. Yang, Z. Chen, X. Song, B. Zhu, T. Hsiai, P.I. Wu, R. Xiong, J. Shi, Y. Chen, Q. Zhou, K.K. Shung, Three dimensional printing of high dielectric capacitor using projection based stereolithography method, Nano Energy 22 (2016) 414–421, https://doi.org/10.1016/j.nanoen.2016.02.045.
[105] Y. Chen, X. Bao, C.M. Wong, J. Cheng, H. Wu, H. Song, X. Ji, S. Wu, PZT ceramics fabricated based on stereolithography for an ultrasound transducer array application, Ceram. Int. 44 (18) (2018) 22725–22730, https://doi.org/10.1016/j.ceramint.2018.09.055.
[106] P. Singh, L.S. Smith, M. Bezdecny, M. Cheverton, J.A. Brewer, V. Venkataramani, Additive manufacturing of PZT-5H piezoceramic for ultrasound transducers, 2011 IEEE International Ultrasonics Symposium (2011 Oct 18) 1111–1114, https://doi.org/10.1109/ULTSYM.2011.0273.
[107] R.J. Huang, Q.G. Jiang, H.D. Wu, Y.H. Li, W.Y. Liu, X.X. Lu, S.H. Wu, Fabrication of complex shaped ceramic parts with surface-oxidized Si3N4 powder via digital light processing based stereolithography method, Ceram. Int. 45 (4) (2019) 5158–5162, https://doi.org/10.1016/j.ceramint.2018.11.116.
[108] H. Ji, H.M. Lim, Y.W. Chang, H. Lee, Comparison of the viscosity of ceramic slurries using a rotational rheometer and a vibrational viscometer, J. Korean. Ceram. Soc. 49 (6) (2012) 542–548, https://doi.org/10.4191/kcers.2012.49.6.542.
[109] S. Song, M. Park, J. Lee, J. Yun, A study on the rheological and mechanical properties of photo-curable ceramic/polymer composites with different silane coupling agents for SLA 3D printing technology, Nanomaterials. 8 (2) (2018) 93, https://doi.org/10.3390/nano8020093.
[110] D.I. Woodward, C.P. Purssell, D.R. Billson, D.A. Hutchins, S.J. Leigh, Additively manufactured piezoelectric devices, Phys. Status. Solidi. A. 212 (10) (2015) 2107–2113, https://doi.org/10.1002/pssa.201532272.
[111] S.P. Gentry, Improving the resolution of manufacturing methods using photo-polymerizable ceramic suspensions, Univ. Mich, 2012 PhD Diss..
[112] G.A. Brady, J.W. Halloran, Solid freeform fabrication of ceramics by stereolithography, Nav. Res. Rev. 50 (1998) 39–43.
[113] J.H. Jang, S. Wang, S.M. Pilgrim, W.A. Schulze, Preparation and characterization of barium titanate suspensions for stereolithography, J. Am. Ceram. Soc. 83 (7) (2000) 1804–1806, https://doi.org/10.1111/j.1151-2916.2000.tb01467.x.
[114] J.H. Lee, R.K. Prud'Homme, I.A. Aksay, Cure depth in photopolymerization: Experiments and theory, J. Mater. Res. 16 (12) (2001) 3536–3544, https://doi.org/10.1557/JMR.2001.0485.
[115] J.H. Lee, R.K. Prud'homme, I.A. Aksay, Processing of organic/inorganic composites by stereolithography, MRS Proceedings 625 (2000) 165, https://doi.org/10.1557/PROC-625-165.
[116] C. Schmidleithner, D.M. Kalaskar, Stereolithography, in: D. Cvetković (Ed.), 3D Printing, IntechOpen, 2018, pp. 1–22, , https://doi.org/10.5772/intechopen.78147.